AED R-3388
January 15, 1969

Final Report for
Laser Tracking and Ranging System

Prepared for:
National Aeronautics and Space Administration
Manned Spacecraft Center
Houston, Texas
In Response To:
Contract No. NAS 9-7482

RCA | Defense Electronic Products
Astro-Electronics Division | Princeton, New Jersey

NASA CR 92485

AED R-3388
January 15, 1969

Final Report for
Laser Tracking and Ranging System

Prepared for:
National Aeronautics and Space Administration
Manned Spacecraft Center
Houston, Texas
In Response To:
Contract No. NAS 9-7482

RCA | Defense Electronic Products
Astro Electronics Division | Princeton, New Jersey

PREFACE

This report describes the development and test of the engineering model of a Laser Tracking and Ranging System constructed by RCA for the Manned Spacecraft Center of the National Aeronautics and Space Administration. Under Contract NAS9-7482, the Astro-Electronics Division of RCA provided project management, designed the Tracking Pedestal Subsystem, with its associated electronic equipment, and performed the system testing. The Advanced Technology Department of RCA's Defense Electronic Products developed the Laser Transmitter and Receiver, and the Range Computer Subsystems. The gallium-arsenide laser diode was developed and supplied by the RCA Laboratories.

TABLE OF CONTENTS

LIST OF ILLUSTRATIONS

LIST OF ILLUSTRATIONS (Continued)

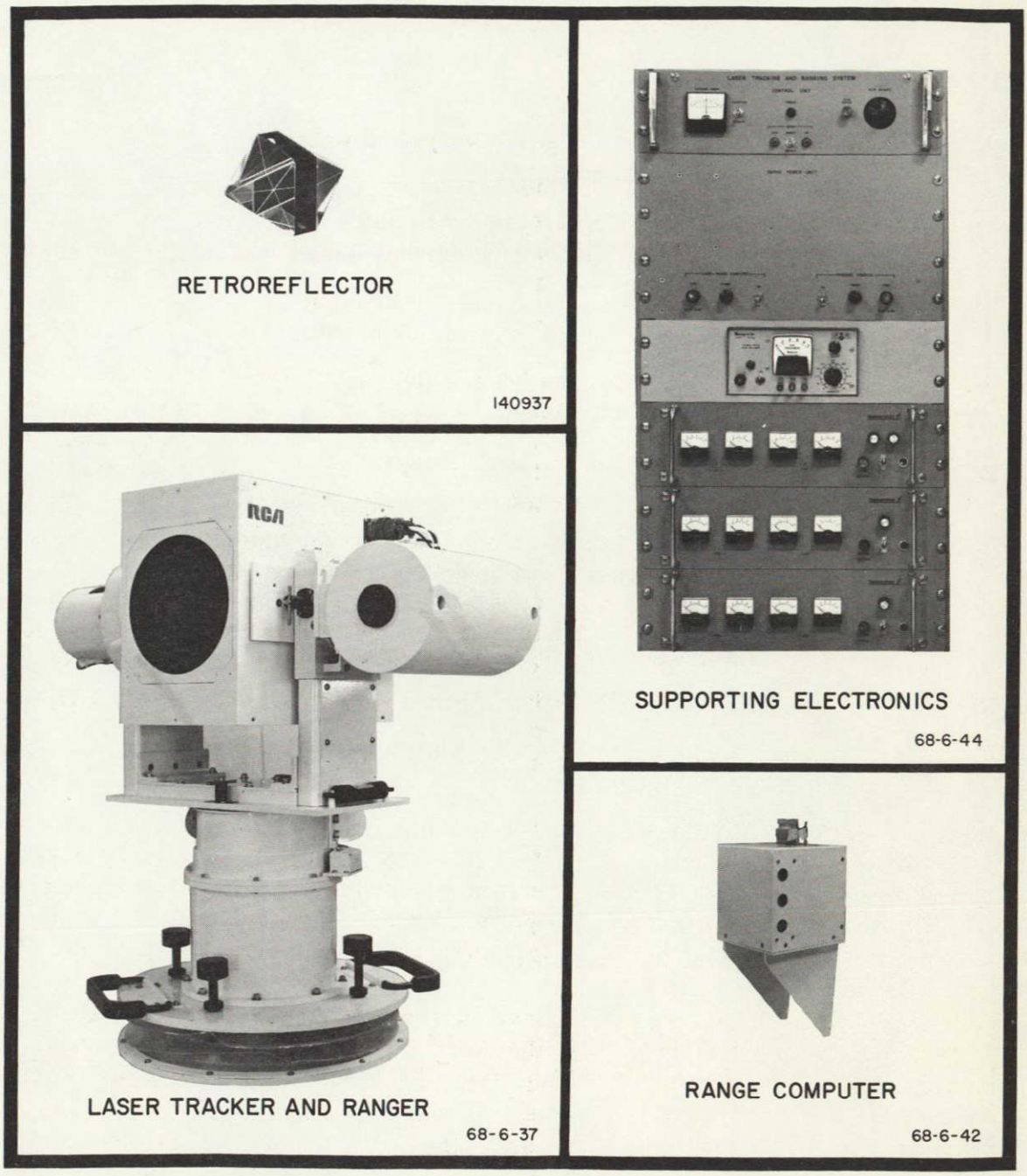

Frontispiece: Components of Laser Tracking and Ranging System

SECTION I. SYSTEM DESCRIPTION

A. INTRODUCTION

The Laser Tracking and Ranging System (LTRS) is an optical tracking radar that uses a gallium-arsenide injection laser as the transmitting source. The system is designed to track a small retrodirective corner-reflector array and to provide continuously the range, azimuth, and elevation of the array's position relative to the tracking unit.

The development effort was directed toward providing a small, compact and relatively lightweight instrument mainly as a part of the Lunar Surveying System for tracking an astronaut's staff. A number of other applications considered include the LTRS as a navigation instrument for a Lunar Flying Vehicle and as a crew safety device for monitoring an astronaut's situation during any EVA operations.

In building The Engineering Model, demonstration of system feasibility and minimum development cost were equally important objectives, so commercial and readily available components whose size and weight are not representative of those in a flight weight configuration were used in many instances. The completed tracking pedestal weighed 45 pounds, but it is estimated that the complete system might weigh only 20 pounds in flight configuration.

The components of the LTRS are shown in the frontispiece. The tracking pedestal contains the laser transmitter, receiver, and servo-driven azimuth and elevation structures. These are supplemented by the rack-mounted servo amplifiers, logic circuits, power supplies, and operating controls. A miniature range computer and the retroreflector array complete the system.

The development project was successful; operational performance met the required specifications. Tracking of the retroreflector target from 12 to 700 meters was demonstrated with azimuth and elevation angular accuracies of ±1 milliradian and a range accuracy of ±1.0 meter. Extension of the range capability to 8000 meters with a ranging accuracy of ±0.5 meter is considered quite possible for a flight instrument.

B. FUNCTIONAL DESCRIPTION

The LTRS is considered as consisting of two major subsystems called, respectively, the Laser/Ranging Subsystem and the Tracking Pedestal

Subsystem. The Laser/Ranging Subsystem includes the transmitting and receiving sections (including the laser diode), the range computer, and the retroreflector array. The Tracking Pedestal Subsystem includes the pedestal structure, the servos, and the acquisition and data-buffering logic. The division of equipment is shown on the System Block Diagram, Figure I-1.

The transmitter incorporates a single large-area injection laser diode. It operates at a repetition rate of 360 pps ±10 percent and provides either a 1 by 5 degree, or a 1 by 3 degree illumination pattern with a pulse duration of 60 nanoseconds. The transmitter peak power output ranges from 3 to 30 watts the level being determined by the value of an AGC voltage applied to a transmitter driver.

The transmitter light pulse is directed towards the retrodirective corner-reflector array, which returns the intercepted light energy to a 5.5 inch telescope at the receiver, as shown in the Optical-Path Diagram, Figure I-2. The received light signal is focused by the telescope mirror onto a quandrant photo-diode The output of each quadrant of the diode is fed into a separate low-noise preamplifier (see Figure I-1) which boosts the signal level to the proper value for the associated amplifier. The four preamplifiers are closely matched with respect to gain and frequency response. Their outputs are fed to AGC amplifiers, which supply the tracking error signals, and also to a summing and differentiating amplifier, which supplies range data.

The four, matched AGC amplifiers feed into four matched peak detectors, and the outputs of the peak detectors are connected to two sum-and-difference amplifiers which provide the azimuth and elevation error signals.

The peak detector outputs are also summed and amplified to provide the AGC control voltage, which determines the AGC amplifier gain and the transmitter output power level.

Azimuth and elevation error signals are amplified in a servo-compensation amplifier and a servo power-amplifier for driving dc torque motors on the azimuth and elevation axes. DC tachometers provide the damping required for stabilization. Optical shaft encoders on both axes provide natural binary readouts of azimuth and elevation.

When the system is not tracking a target, or if a target track is lost, the system may be made to enter an acquisition scan program which consists of sweeping the tracker line of sight from side to side (that is, about the azimuth axis) between increasing limits. In this mode, if a target falls within the tracker field of view, the system will immediately lock onto and track the target.

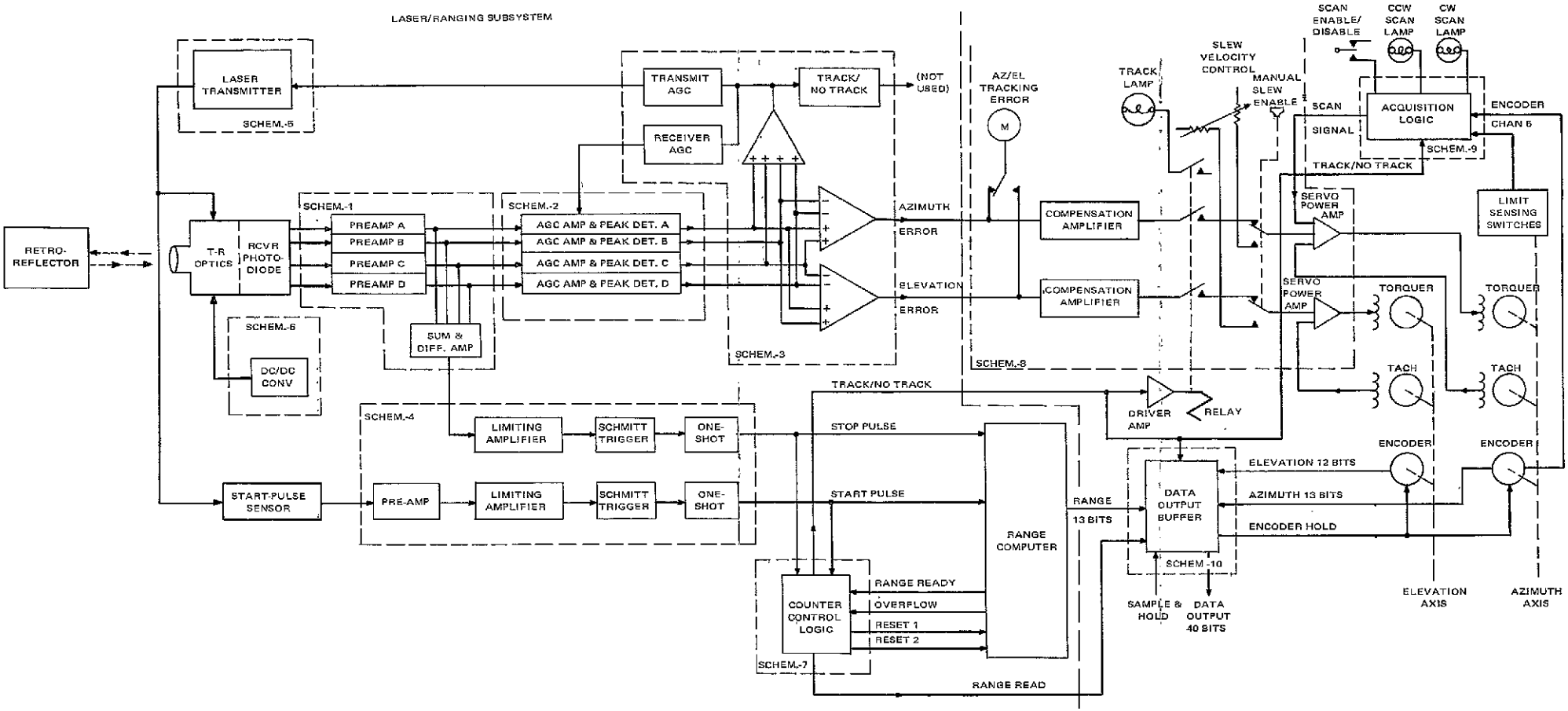

Figure I-1. Laser Tracking and Ranging System, Block Diagram

FOLDOUT FRAME /

FOLDOUT FRAME 2

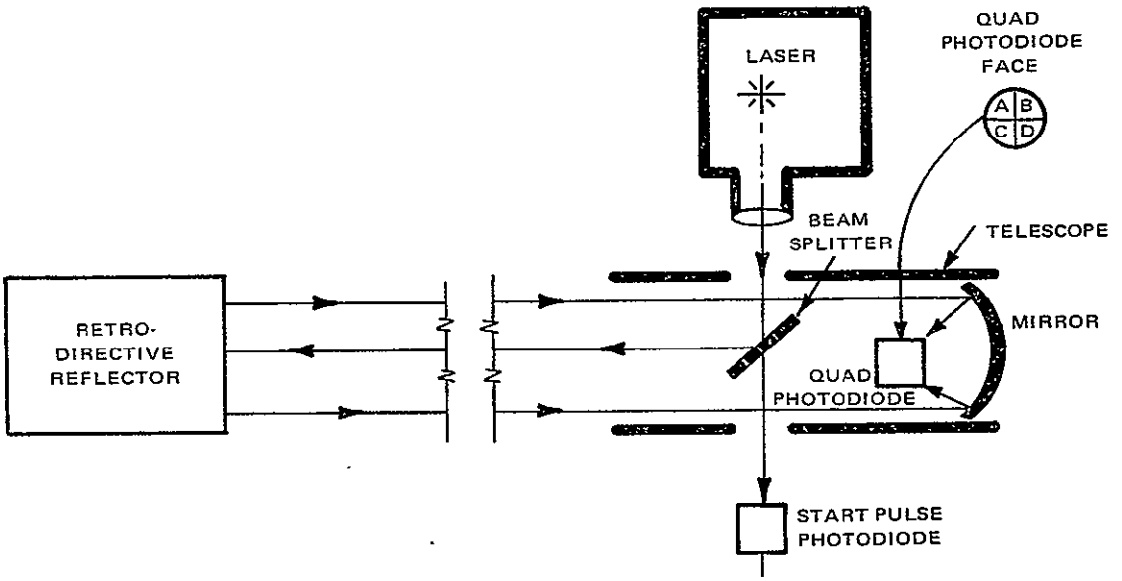

Figure I-2. Optical Path Diagram

Range data are obtained from a range computer that measures the time interval between the transmitted pulse and the received pulse. This computer normally averages the values of 32 range measurements, but has provisions for averaging the results from 1, 2, 4, 8, or 16 measurements as well. A range "read" signal is generated only if all measurements are less than 1536 meters, permitting transfer of the data to the data output circuits; otherwise, an overflow condition is sensed which inhibits the transfer control signal.

The "start" pulse for the range computer is obtained by sampling a small portion of the transmitted light pulse with a photodiode. The output of the photodiode is passed through a preamplifier and is differentiated to yield a signal whose zero crossing corresponds to the peak of the transmitted pulse. This signal is passed through a limiting amplifier which clips the peaks of the differentiated signal but does not disturb the zero crossing. A Schmitt Trigger senses this zero crossing and triggers a monostable (one-shot) multivibrator which generates a very sharp pulse for starting the range computer count.

The range computer is stopped at the appropriate time by a signal obtained from summing and differentiating the four receiver preamplifier outputs. This differentiated signal is then amplified and limited. The limited signal is sensed with a Schmitt Trigger, which triggers a one-shot multivibrator, thus stopping the range computer count. The pulse-forming circuits for starting and stopping the range counter are matched as closely as possible in order to cancel time-shift errors due to temperature and other effects.

C. DEVELOPMENT HIGHLIGHTS

The RCA Astro-Electronics Division (AED) solicited the assistance of other RCA facilities for specialized requirements in the development of the Laser Tracking and Ranging System. The transmitter-receiver electronics and optics, and the range computer, were developed by the Advanced Technology Department of RCA. The gallium-arsenide laser diode was developed and supplied by RCA Laboratories. AED coordinated the system development, designed the tracking pedestal, the servos, and the acquisition and data buffering logic, and integrated and tested the complete system.

The wide-area, gallium-arsenide laser diode, now being produced in small (prototype) quantities by the RCA Laboratories, has a typical lasing threshold of 90 amperes and a typical power output of 35 watts at three times threshold, with uniform lasing along the diode junction. The diodes initially supplied by the Laboratories provided reasonably uniform lasing down to 1.5 times the threshold current; below this value, portions of the junctions ceased to lase. It then appeared that 1.5 times threshold was the lower limit on AGC control. This corresponds to approximately a 5 to 1 control ratio for the transmitted power.

However, as laser development progressed at the Laboratories, wide-area diodes with excellent uniformity of the lasing junction down to 1.2 times threshold were produced. This permitted an increase in the AGC control ratio to the desired 10 to 1 range with no degradation of the transmitted far-field pattern.

One diode obtained lased uniformly down to 1.2 times threshold current, with only a slight dimming of a portion of its junction at that value; this diode was selected for incorporation into the LTRS engineering model.

Conservative approaches were used in both system and circuit designs to improve the likelihood of meeting all technical requirements. The use of automatic gain control in the ranging circuits was given up at the start of a limiting technique for handling the wide variations of signal input level without introducing timing errors. Also, the ranging computer was designed with the capability of averaging the values of up to 32 individual range measurements, so that random range timing errors could be substantially reduced. These approaches gave very satisfactory performance in the ranging system and the range accuracy specification of ±1.0 meter was met without the degree of difficulty initially expected.

A survey of manufacturers of tracking pedestals was made to see if a suitable unit could be procured for the LTRS. The products of two companies nearly met the requirements: those of Aeroflex, on Long Island, and Scientific-Atlanta of Atlanta, Georgia. It was determined that the Aeroflex unit was too

large and could not be delivered within a reasonable schedule. The Scientific-Atlanta unit met all requirements except that it weighed 80 pounds and represented a departure in design concept from the originally proposed version. After discussions with Manned Spacecraft Center personnel, it was decided that a more favorable design would result if RCA would build the tracking pedestal.

One change in the originally proposed pedestal design resulted from the large number of circuits that were required to go through the azimuth axis. An azimuth shaft encoder having an annular rather than conventional construction was used, enabling wires to be fed through its center. A second change from the proposal configuration was a yoke configuration for the elevation axis, with the laser unit within the yoke and the surveillance camera and elevation drive cantilevered from opposite sides. The advantages of this configuration are: (1) it minimizes the azimuth moment of inertia, (2) it provides better support, and (3) it simplifies the elevation axis drive.

The Laser/Ranging Subsystem was completed and tested first to demonstrate range capability, ranging accuracy, and electrical boresight accuracy as a function of range. The system was then completely integrated and testing of the system functioning and performance was carried out. System performance was tested using a specially surveyed range having seven stations, located from 12 meters to 700 meters from the instrument station. Testing on this range verified range capability, tracking capability, range and angle tracking accuracies, and reacquisition capability.

Temperature and vibration environmental tests were made on the non-operating tracking pedestal to assure that the unit would survive conditions and rough handling in the field. For the vibration test, the tracking pedestal was placed in its specially designed shock isolating carrying container and both container and pedestal were vibrated. No damage resulted from the environmental testing, except for one wire connection which broke off during vibration.

After all system and environmental tests were complete, the LTRS was shipped to the NASA Manned Space Flight Center in Houston. There, after some minor difficulties, the performance level of the unit was verified again.

SECTION II. SYSTEM ANALYSIS

Studies were conducted to determine the transmitter power required for operation of the LTRS at a range of 700 meters, to show that a cluster of eight corner-cube reflectors satisfies the requirement for an omnidirectional retrodirective reflector, and to confirm that the energy density of the laser beam is sufficiently low that it can be intercepted safely by the human eye.

A. SIGNAL-POWER ANALYSIS

An analysis was made to determine the transmitter output power required to provide the laser system with a range accuracy of ±0.5 meter at a range of 700 meters. The minimum received signal power required is determined by evaluating the minimum signal-to-noise ratio required for ±0.5 meter accuracy and the noise contribution of the detection circuitry. The minimum transmitter output power is then determined from this minimum required received power and the transmission characteristics of the operating media.

At the maximum range of 700 meters, the received light pulse will be contaminated with noise and a timing error will be introduced in the zero crossing of the differentiated signal. This timing error is given by:

$$t_e = \frac{1}{2\,B\,\sqrt{SNR}}$$

Since the timing error, t_e, corresponds to the round trip transmission time, the corresponding range error, ℓ_e, is given by:

$$\ell_e = \frac{c\,t_e}{2}$$

where c is the transmission velocity.

Substituting for t_e yields,

$$\ell_e = \frac{c}{4\,B\,\sqrt{SNR}}$$

and

$$SNR = \frac{c^2}{16\, B^2\, \ell_e}$$

For an amplifier having a Gaussian frequency response (i.e., the response of an amplifier containing a large number of simple RC-type roll-off stages) the bandwidth for maximum SNR is given by:

$$B = 0.4/\tau$$

where τ is the pulse duration of the received signal.

For a pulse duration of 60 nanoseconds, B = 7 MHz and the signal-to-noise ratio required for ±0.5 meter accuracy is 460, or 26.6 dB.

For the photodiode receiver used in the LTRS, the minimum received signal power required is given by:

$$P_s = \sqrt{(SNR)\, \frac{2e\, B\, \rho\, P_b\, R_L + 2\, FKTB}{\rho^2\, R_L}}$$

where

SNR = required signal-to-noise ratio (= 460)

e = charge on an electron (= 1.6×10^{-19} coulomb)

B = receiver bandwidth (= 7 MHz)

P_b = background power

ρ = photodiode responsivity (= 0.5 ampere/watt)

R_L = photodetector load resistance

F = receiver noise figure (= 4 (measured))

K = Boltzmann's constant (= 1.38×10^{-23} Joule/°K)

T = receiver temperature (= 300°K)

The load resistance on the photodiode is determined from the load capacitance and the bandwidth. For a load capacitance of 76 pF (photodiode capacitance of 70 pF and stray capacitance of 6 pF) and a 7-MHz bandwidth,

$$R_L = 300$$

The value of P_b, the background power due to sunlight is given by:

$$P_b = \frac{M\gamma_h \gamma_v A_r \xi T_o B_f}{\pi}$$

where

M = solar irradiance at 9000 Å (= 0.1 watt/m^2/Å)

ξ = background reflection coefficient [= 1.0 (worst case)]

γ_v = vertical transmitter beamwidth (= 87.5 milliradians)

γ_h = horizontal transmitter beamwidth (= 17.5 milliradians)

A_r = area of receiver aperture (minus blockage) (= 1.33×10^{-2} m^2)

T_o = optical system transmission (= 0.7)

B_f = optical filter bandwidth (= 200 Å)

$$P_b = 9.6 \times 10^{-5} \text{ watt}$$

The value for P_s can then be calculated to be

$$P_s = 1.28 \times 10^{-6} \text{ watt}$$

The minimum transmitter power required to produce a received signal power of 1.28 microwatts from a retroreflective target at 700 meters can now be calculated. The required transmitter power is determined by assuming that the transmitted beam passes through an aperture having the same diameter as the retroreflector and is collected by a fictitious receiver located at twice the distance from the transmitter to the receiver. The equivalent geometry is shown in Figure II-1.

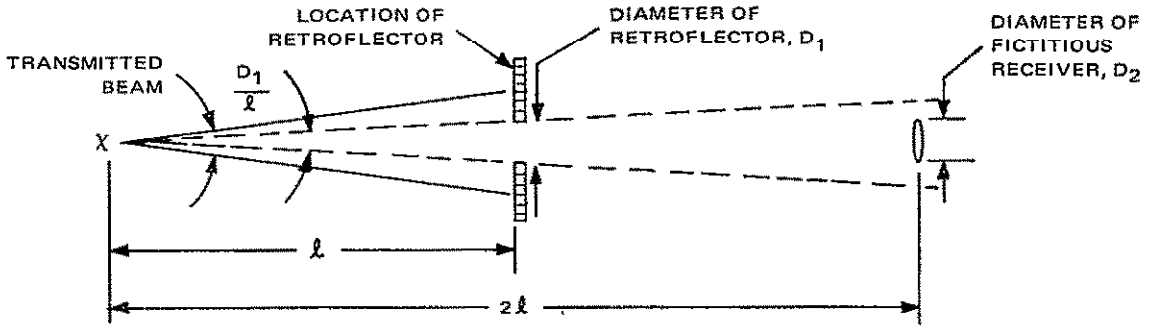

Figure II-1. Equivalent Geometry of Retroreflector System

Two factors complicate this geometry. The first is caused by diffraction of the beam returned to the LTRS from the retroreflector. As the range increases, the width of the reflected beam, D_1/R, decreases. There is, however, a lower limit of reflected beam width caused by diffraction, which is equal to $122\lambda/D_1$.

The other factor is caused by aperture blockage of the receiver, due to the photodetector and telescope reflector structure. This effect varies with the size of the retroreflector, and may also vary with range if the retroreflector diffraction is appreciable.

From the simple geometric relationships and corrections for diffraction limits of the retroreflector, and blockage of the receiver preamplifier housing, the required transmitter power is given by:

$$P_t = \left[\frac{\pi P_s \gamma_h \gamma_v \ell^2}{4 T_o' A_{tgt}}\right] \left[1 - \frac{4 A_b \ell}{\pi} \left(\frac{1}{2D_1 + \frac{122 \lambda_B \ell}{D_1}}\right)^2\right]^{-1}$$

where

P_t = peak transmitter power

γ_h = horizontal transmitter beamwidth (= 17.5 milliradians)

γ_v = vertical transmitter beamwidth (= 87.5 milliradians)

ℓ = range (= 700 meters)

A_{tgt} = effective area of retroreflector (= 5.05×10^{-4} meter^2)

D_1 = diameter of retroreflector (= 2.54×10^{-2} meter)

P_s = minimum signal power required (= 1.28×10^{-6} watt)

T_o' = transmission of total optical system (= 0.4)

$A_{b\ell}$ = blocking area of preamp. housing (= 2.09×10^{-3} meter^2)

λ_B = wavelength of transmitted beam (= 9180 Å)

Solving the equation,

$$P_t = 6.2 \text{ watts}$$

The transmission equation used above is valid for no atmospheric attenuation or turbulence. While this ideal transmission would be realized on the surface of the moon, conditions on the earth's surface where the engineering model tests are performed, are not.

B. RETRODIRECTIVE REFLECTOR DESIGN

The retrodirective reflector (or retroreflector) array is a cluster of eight small corner-cube reflectors (glass pyramids) arranged so that the entry/exit facets form a regular octahedron. The analysis below shows that there is a relatively small variation in the retrodirective cross-section as a function of look-angle for this array. Figure II-2 gives the relative cross-section area of a single reflector as a function of look-angle, ϕ, from the entry/exit facet normal for two direction angles, θ, from the normal: direction θ_1 from the normal to an edge bisector and direction θ_2 from the normal to an apex. Curves for all other direction angles will fall between the two. An open reflector has a zero cross-section at the edge bisector and the apex (for reflection from three surfaces). The glass reflector has a refractive index of about 1.5, giving a relative cross-section of 0.535 and 0.235 for look-angles at the edge bisector and the apex, respectively.

The actual retrodirective cross-section for a single reflector and two views of an octahedron array is shown in Figure II-3. The light (unshaded) portion is the actual cross-section. If the cross-section area of a single reflector, viewed along the facet normal, is taken to be 1.0, the cross-sections of view B is 1.07

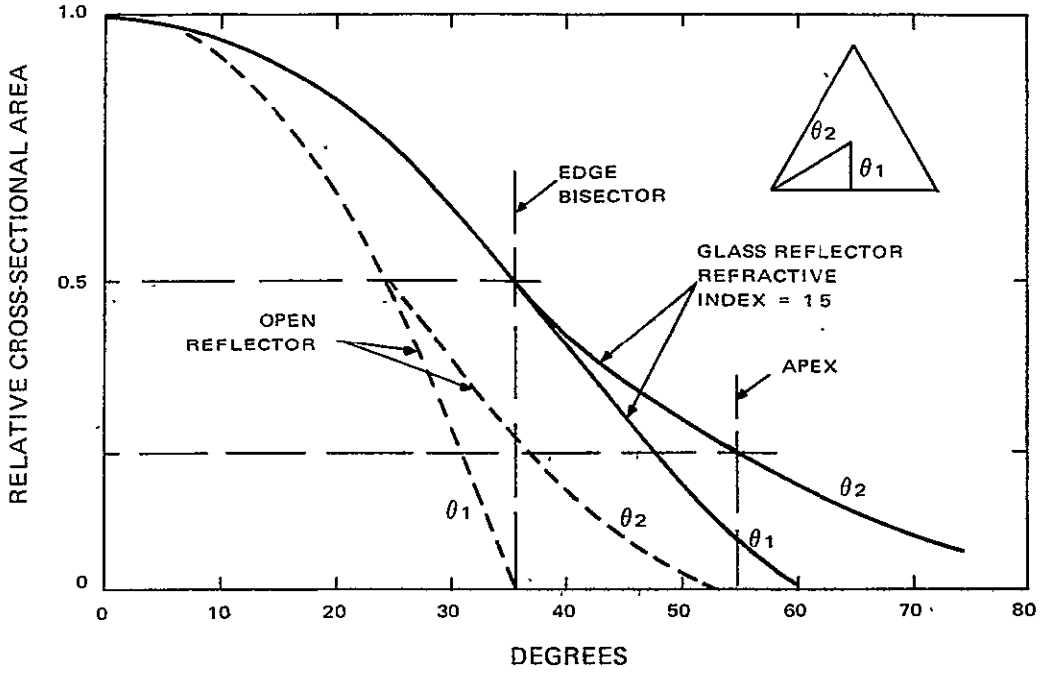

Figure II-2. Retrodirective Cross-Section of a Corner Cube Reflector versus Off-Axis Angle

and that of view C is 0.94. Considering the symmetry of the octahedron, which has 8 facets, 12 edges and 6 apexes, the above values represent 26 well-distributed look angles into the retroreflector array. It is concluded that the cross-section area variation is small and well represented by the cross-section of a single reflector, viewed along the entry-exit facet normal.

To produce a 1-inch diameter effective cross-section, the entry/exit facet was sized to inscribe a 1-inch diameter circle, as shown in Figure II-4. This produces an array with close to a 1-inch diameter retrodirective cross-section for any look angle.

C. EYE SAFETY CONSIDERATIONS

A study made previously by RCA showed that a laser beam with the same energy density as in the proposed design would produce an energy density on the retina of the eye that was 100 times below the threshold at which retinal coagulation can take place. The calculation assumed that the entire beam entered the eye at close range and was focused on the retina.

Since that time, the Army Material Command has issued guidelines that state the safe level of operation is an energy density of 0.1 microjoule/cm^2 or less at the cornea of the eye.

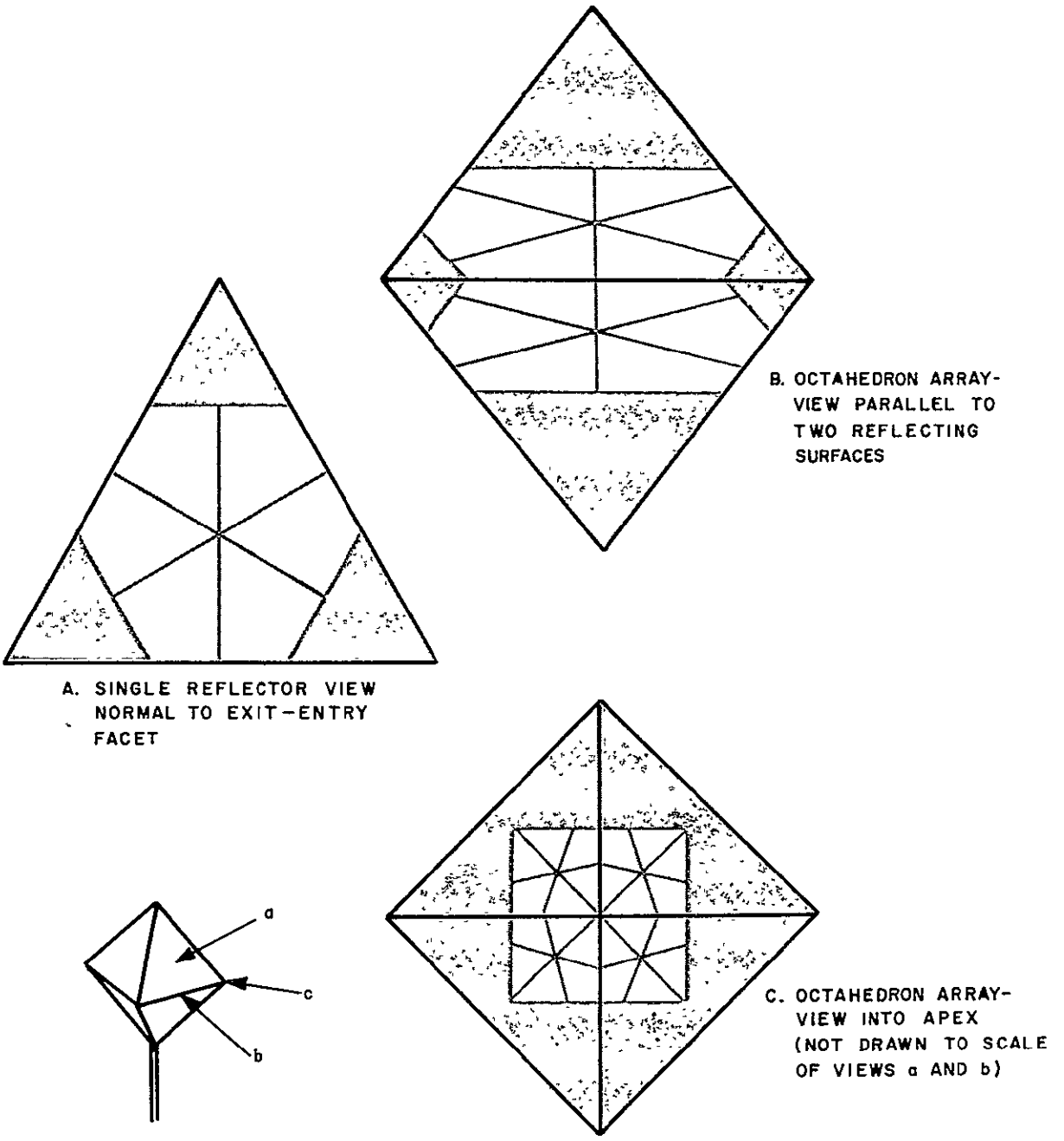

Figure II-3. Retrodirective Cross-Section for Three Viewing Angles

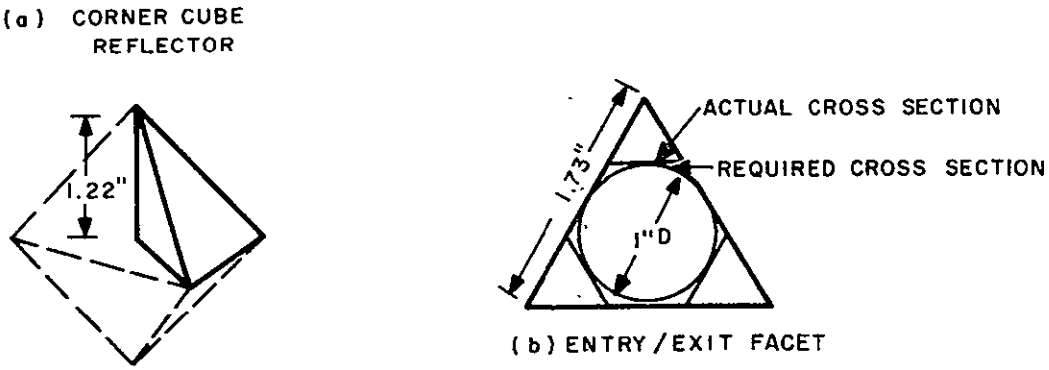

Figure II-4. Geometry of Corner-Cube Reflector

Assuming there is no AGC control of the laser output, the energy per pulse, E/p, is determined by:

$$E/p = P_t \tau$$

where

P_t = peak transmitter power (= 25 watts)

τ = pulse width (= 60 nanoseconds).

Therefore,

$$E/p = 1.5 \times 10^6 \text{ joule/pulse}$$

If the laser energy is spread uniformly over the entire cross-section of the beam, the smallest safe cross-sectional area is 15 cm^2. For a beam pattern of 1 by 5 degrees, the beam will have this cross-sectional area at a range of 0.99 meter. Thus, if the full 25-watt power were used, optic interception would be safe at any range beyond 1 meter. However, since the transmitter will be AGC controlled, the diffuse backscatter from any near object would cause a reduction of transmitter power to less than 3 watts, reducing the maximum safe distance to about 30 centimeters.

For a 3-year period, RCA has conducted a program of periodic eye examinations for all personnel working with lasers. The results have shown not a single case of any detectable eye damage associated with the laser work. It may be concluded, therefore, on the basis of calculations, guidelines, and experience, that operations with the Laser Tracking and Ranging System may be carried out safely without the need for eye protection.

SECTION III. LASER/RANGING SUBSYSTEM

The Laser/Ranging subsystem comprises the transmitter-receiver unit and the range computer. The former includes the optics and the retrodirective reflector. The range computer consists of an interpolating time-interval counter and control circuitry that permits averaging of measurements. It was supplied to RCA by Nanofast, Inc.

A. ELECTRONIC COMPONENTS

1. Transmitter

The transmitter is designed around the laser diode and optical assembly, and a drive circuit capable of providing 300-ampere, 75-nanosecond pulses at a 360-pps rate for driving the laser diode.

The laser diode assembly is shown in simplified form in Figure III-1. Since the laser radiates directly a narrow, rectangular beam, a lens system was selected

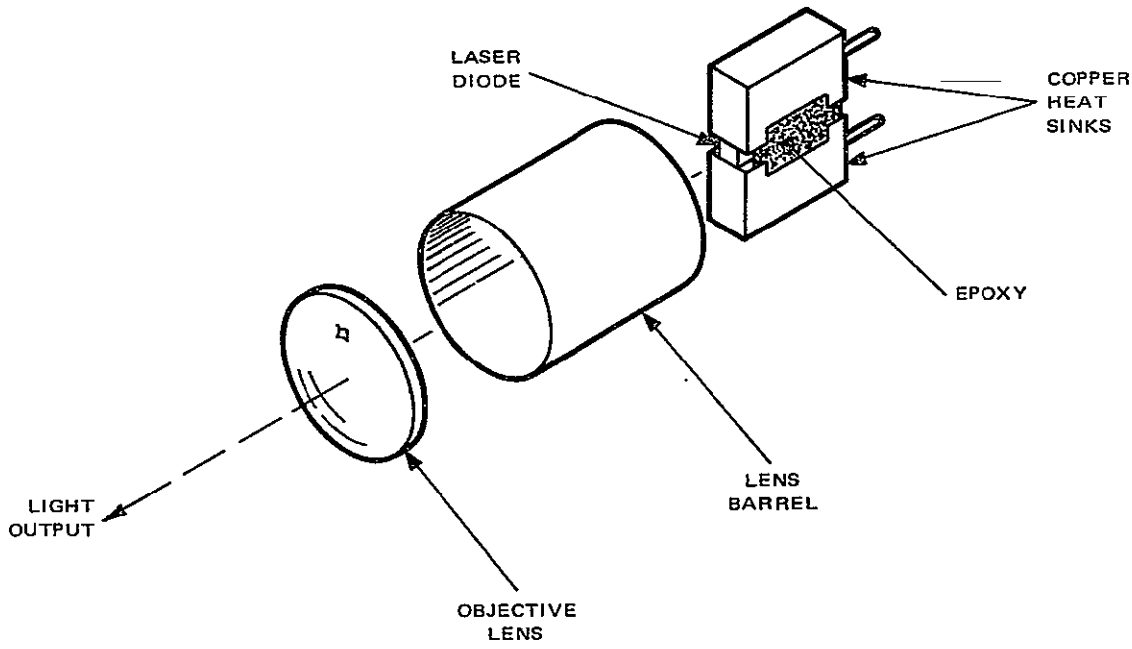

Figure III-1. Laser Optical Assembly

to produce either the 1 × 5 degree or 1 × 3 degree beam required for the laser system. A convex objective lens, slightly defocused, provides a basic 1 × 3 degree output pattern. A supplementary cylindrical lens in a removable assembly is used to spread the vertical angle to 5 degrees if the 1 × 5 degree pattern is desired.

The transmitter driver incorporates a unijunction transistor oscillator which triggers an SCR driver stage which in turn triggers three parallel SCR output drivers (see Figure III-2). Current pulses of the required characteristics are obtained when the three output SCR's discharge the three 9900 picofarad capacitors through the laser diode. Between pulses these capacitors charge up through the 82 kilohm resistors. The 50-kilohm potentiometer is used to adjust the transmitter frequency from 324 to 396 pulses per second. The output power from the transmitter is controlled by changing the voltage applied to the 82-kilohm resistors. The AGC control signal is a current which can be varied, depending on received signal strength, from zero to 0.5 milliampere. This current, flowing through the 330-kilohm resistor and the 500-kilohm potentiometer, varies the voltage applied to the 82-kilohm resistors between 560 volts and 300 volts. This change varies the output power from 30 watts to 3 watts.

A photograph of the laser transmitter is shown in Figure III-3. The subassembly at the right side of the unit is the mount and heat sink for the three driver SCR's and the laser diode. The light output is in a direction corresponding to looking into the page.

Figure III-4 shows a plot of transmitter output power versus the AGC control voltage into the transmitter circuit. The inset shows an oscillogram of the power output at a control potential of 500 volts.

The power was measured at the output of the transmitter mirror with a calibrated photodiode detector. The curve shows how the transmitter output can be controlled from a maximum of 31 watts to a minimum of less than one watt. At the very low output levels, the junction of the laser diode is partially shut off, but system operation is still good. Operating beyond the 560-volt level could cause the laser diode to overheat and fail.

2. Receiver

a. Optics and Photodiode Sensor

The receiver incorporates reflecting optics to focus the returned laser beam on a quadrant photodiode. The four amplified outputs from the photodiode generate the signals for both tracking and ranging. For tracking, the photodiode outputs are processed to obtain the azimuth and elevation tracking errors. For ranging, the outputs are summed together and differentiated for accurately obtaining the timing of maximum pulse amplitude.

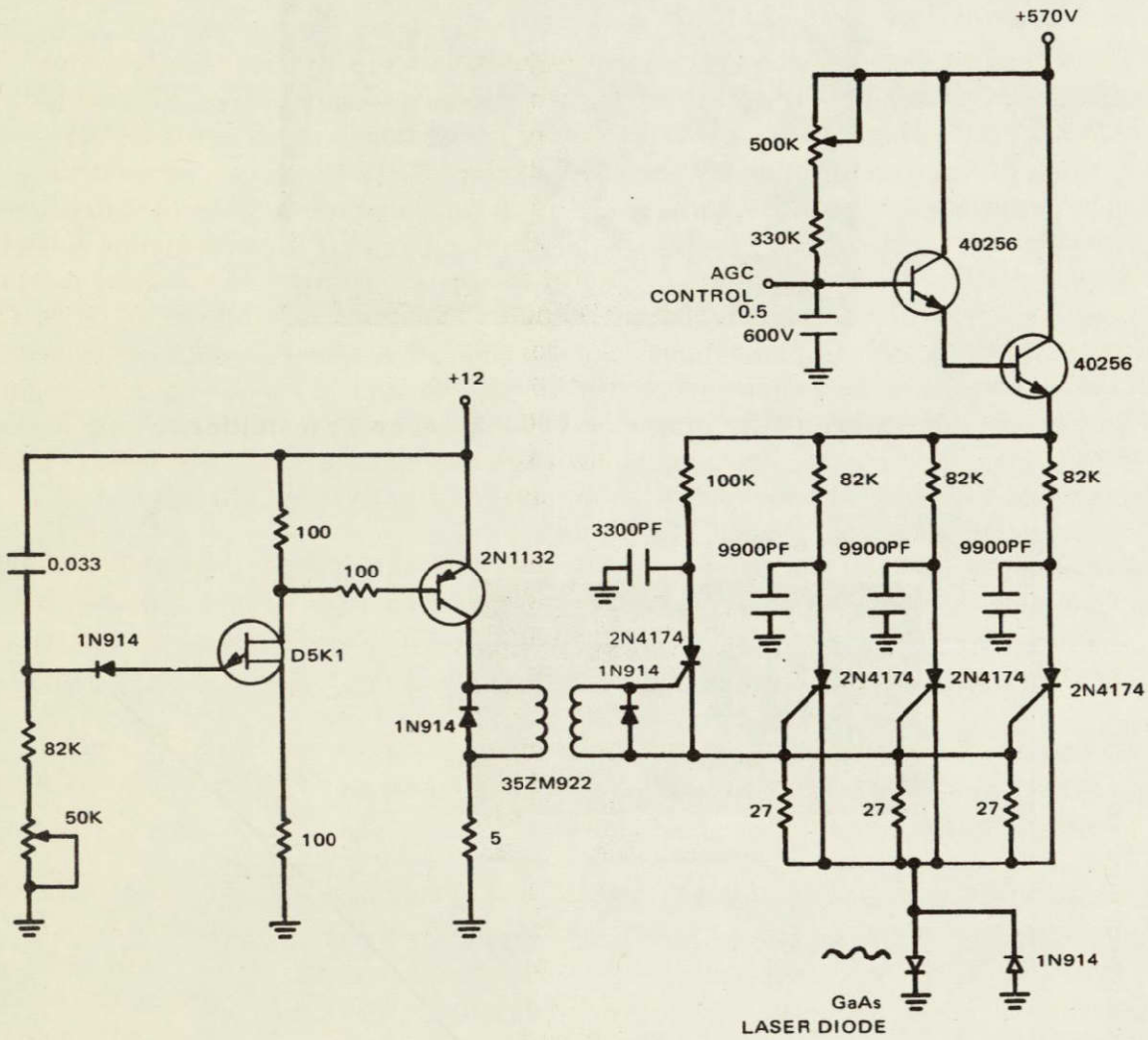

CAPACITANCE IS μF, RESISTANCE IS
OHMS UNLESS OTHERWISE SPECIFIED.

Figure 3-2. Laser Transmitter, Schematic Diagram (Schematic 5)

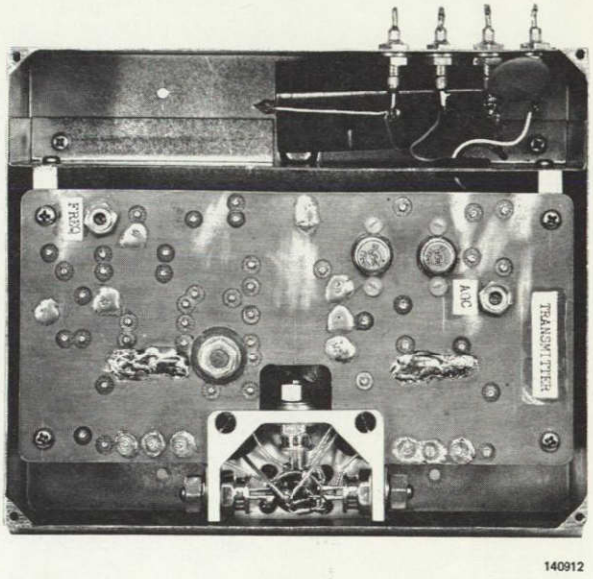

Figure III-3. Interior View of Laser Transmitter

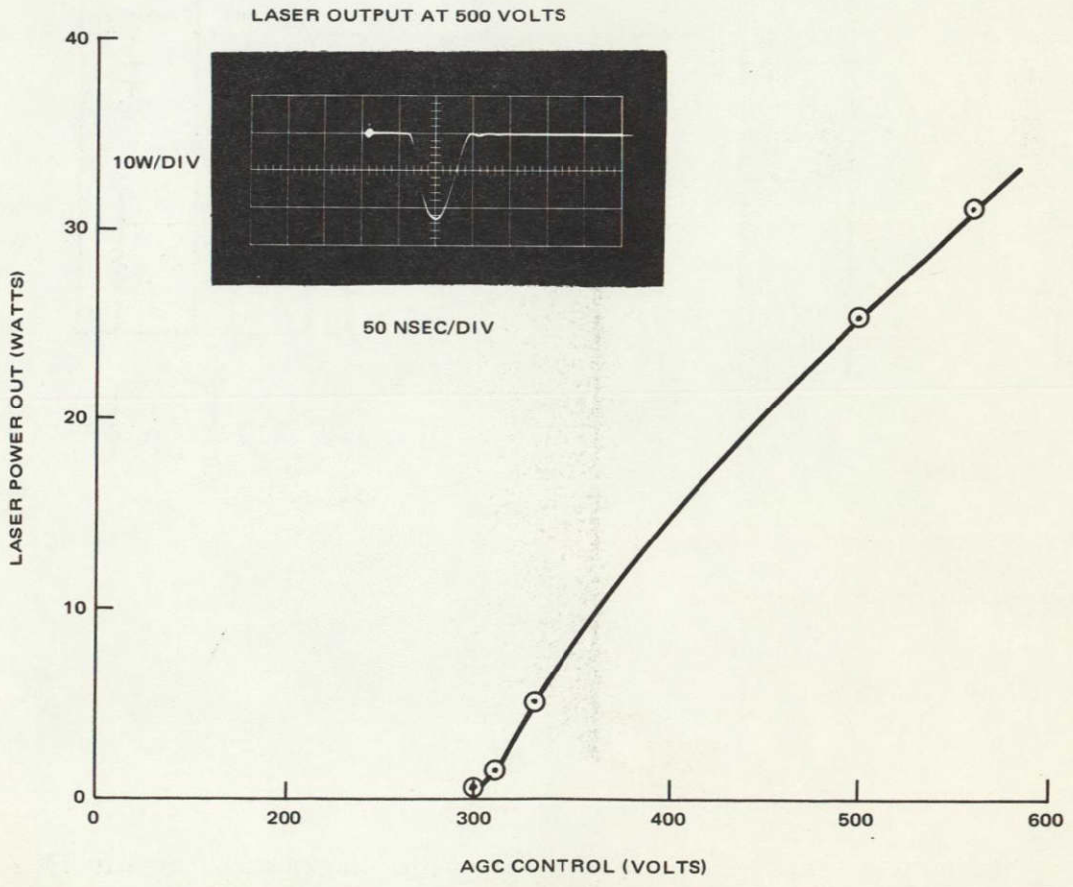

Figure III-4. Effect of AGC Control Voltage on Laser Transmitter Output, Curve

b. Receiver Preamplifiers

A close-up view of the preamplifier assembly is shown in Figure III-5. This assembly includes the receiver quad photodiode (SGD 444-4), four matched preamplifiers, and the sum and differentiator circuit. The circuit diagram for this assembly and an oscillogram showing the four preamplifier outputs and the sum and differentiator output is shown in Figure III-6. These output signals correspond to what would be obtained at a range of about 50 meters. The preamplifier circuit is essentially a low-noise pnp common-emitter stage (for voltage gain) with an npn emitter-follower output stage to buffer the gain stage from the preamplifier loads. The input impedance of the preamplifier is designed to use the photodiode capacitance (plus stray circuit capacitance) and the input resistance as a low-pass network with a cutoff frequency of 7 megahertz. This bandwidth provides optimum signal-to-noise ratio for a system using 60-nanosecond-wide pulses. Each preamplifier has a gain of 12 millivolts per microwatt of photodiode illumination and can handle up to 400 microwatts of input power.

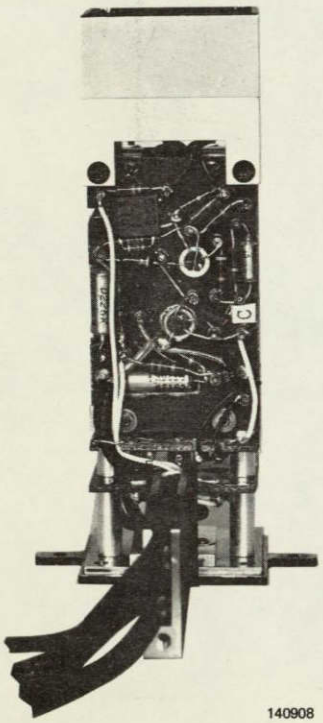

Figure III-5. Preamplifier Assembly, View of Chassis

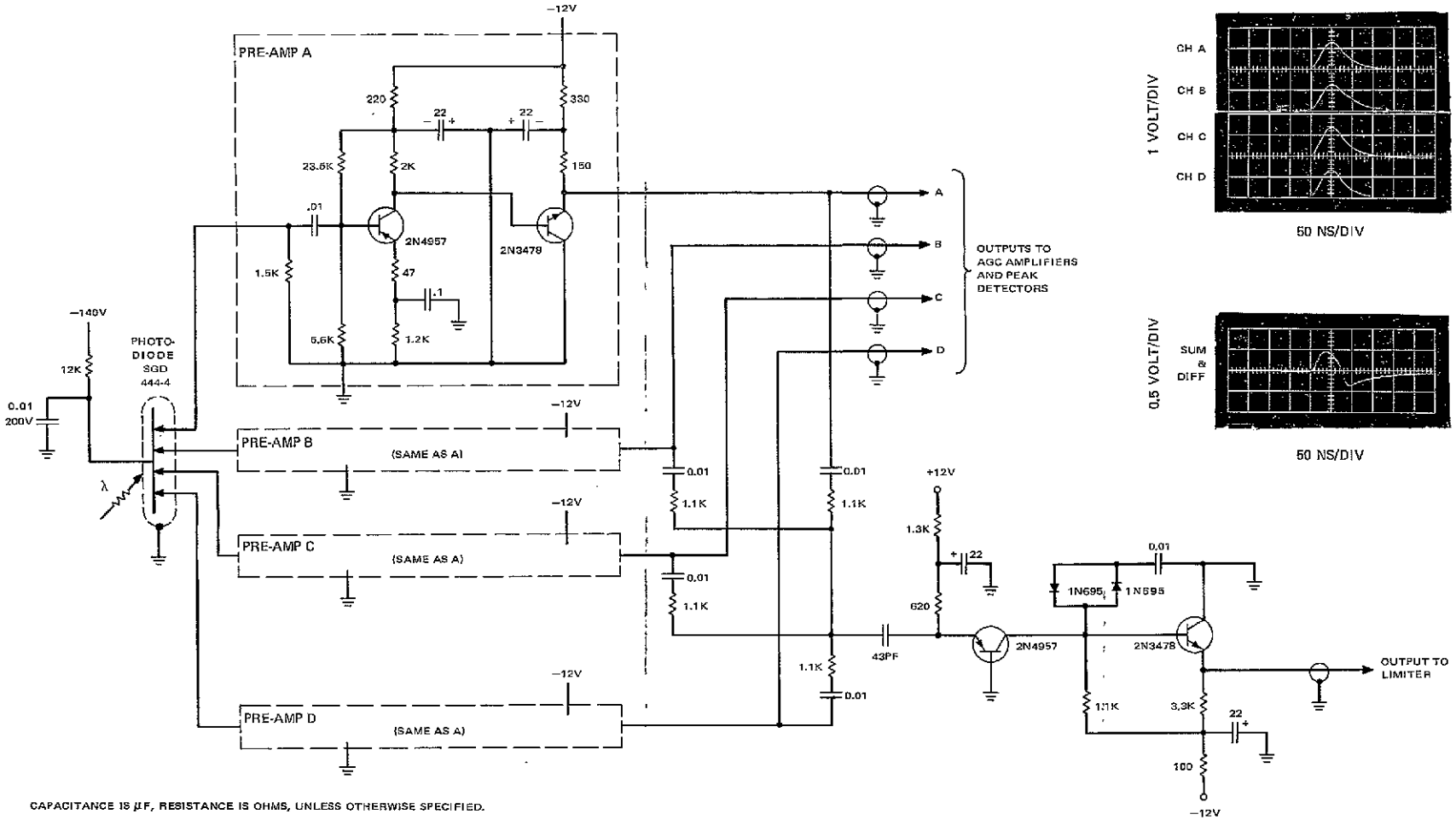

CAPACITANCE IS μF, RESISTANCE IS OHMS, UNLESS OTHERWISE SPECIFIED.

Figure III-6. Receiver Preamplifier Assembly, Schematic Diagram (Schematic 1)

FOLDOUT FRAME

FOLDOUT FRAME 2

The input portion of the sum and differentiator circuit is a resistor-summing network which drives a differentiating capacitor. The current through the capacitor flows into the low-impedance pnp common-base stage. This same current flows into the collector load resistor of the common-base stage, producing a voltage swing which represents the differentiated sum of the preamplifier outputs. The back-to-back diodes in the collector circuit provide clipping which limits the maximum output to about ±0.4 volt. The emitter-follower output stage prevents the collector circuit from being affected by the output load. The sum and differentiator can handle pulses up to 4 volts in amplitude on all four of its inputs without producing any time shift in the zero crossing of the output signal.

A dc-to-dc converter is used to supply the -140-volt bias to the receiver quadrant photodiode. The circuit diagram for the converter is shown in Figure III-7. The circuit is essentially a unijunction oscillator with a power-output stage coupled through step-up transformer. The high-voltage pulses from the secondary of the transformer are rectified, filtered, and Zener-diode regulated to produce the proper high-voltage dc output. The circuit operates at a frequency of about 10 kHz.

c. Tracking Circuitry

The tracking circuits comprise four AGC amplifiers and peak detectors, an AGC control amplifier, and two amplifiers for deriving azimuth and elevation tracking errors.

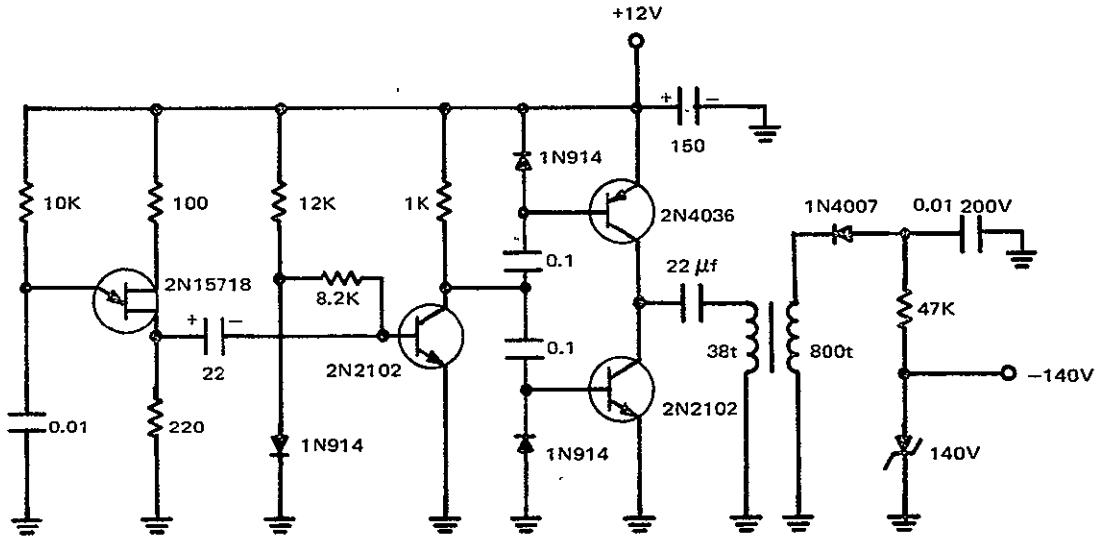

CAPACITANCE IS µF, RESISTANCE IS OHMS, UNLESS OTHER SPECIFIED.

Figure III-7. DC-to-DC Converter, Schematic Diagram (Schematic 6)

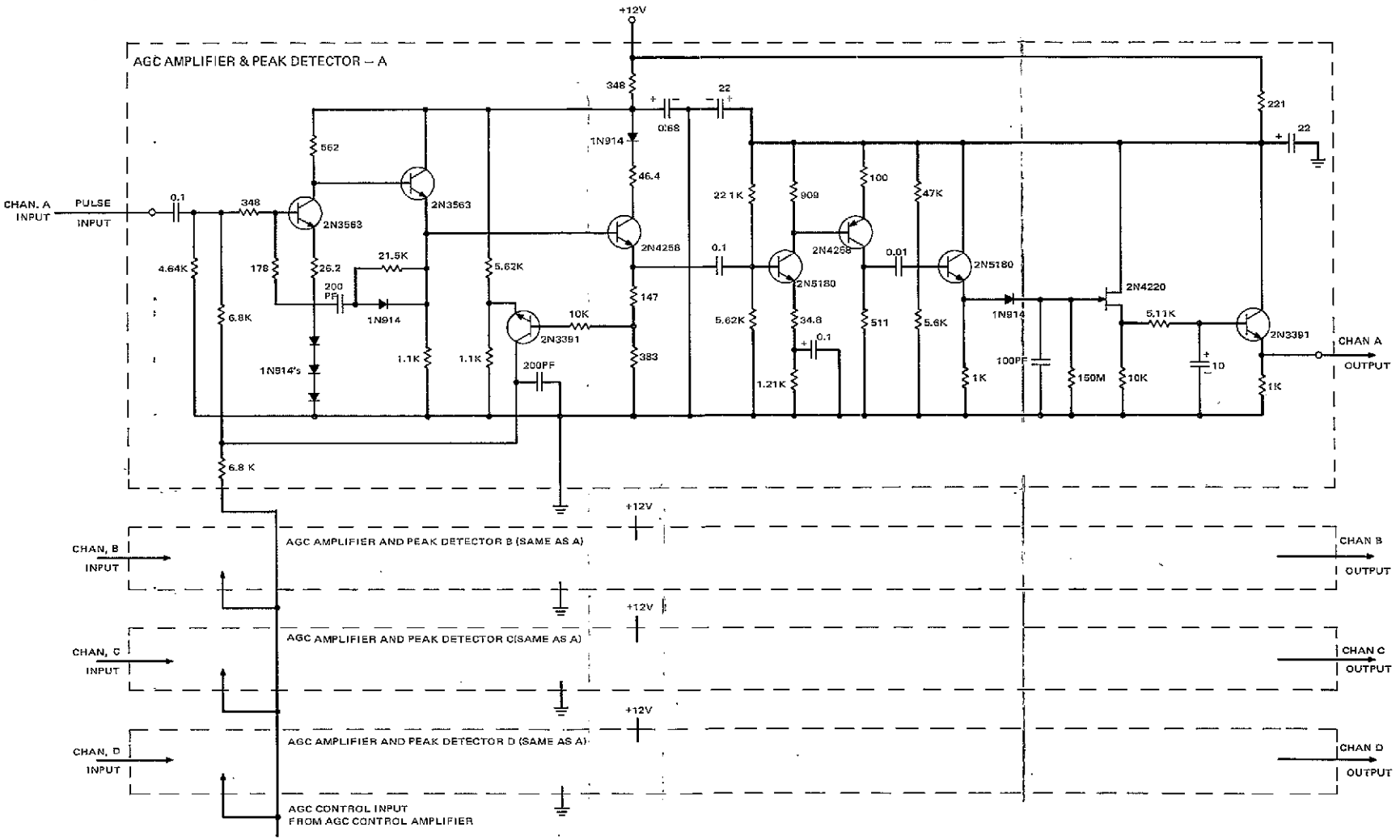

CAPACITANCE IS μF, RESISTANCE IS OHMS, UNLESS OTHERWISE SPECIFIED.

Figure III-8. AGC Preamplifiers and Peak Detectors, Schematic Diagram (Schematic 2)

FOLDOUT FRAME 1

FOLDOUT FRAME 2

(1) AGC Amplifier and Peak Detector Stages

The circuit diagram for the AGC amplifier and peak detector is shown in Figure III-8. The AGC amplifier consists of an npn common-emitter stage with an emitter-follower output that drives a pnp common-emitter output stage. Gain control is accomplished by varying the dynamic impedance of the diodes in the emitter circuits of the npn and pnp common-emitter stages. The AGC input controls the dc current which flows through the diodes. The dynamic impedance of the diodes varies with this dc current. By adjusting the control input from 2 to 11 volts, a constant-pulse output of 60 millivolts can be obtained while the pulse input is varied from 3 volts to 3 millivolts. The transistor connected into the output resistor network prevents the AGC control input from causing amplifier saturation at the high control level.

The peak detector circuit contains a complementary npn-pnp amplifier stage with an emitter-follower output. This amplifier stage boosts the 60-millivolt pulse from the AGC amplifier to a level of about 3 volts. The 100-picofarad capacitor is charged to the peak of this 3-volt pulse through a diode. The leakage current of the FET source follower and the 150-megohm resistor, as well as the leakage current of the charging diode, serve to discharge the 100-picofarad capacitor. The charging and discharging time constants are about 50 nanoseconds and 10 milliseconds, respectively. The FET source follower drives the emitter-follower output stage through a resistor-capacitor lag network. This network provides the necessary compensation to keep the closed-loop AGC system stable.

One of the four AGC Amplifier and Peak Detector boards is shown in Figure III-9 (a). Precision resistors and matched diodes and transistors have been used for this circuitry to provide close channel-to-channel matching. Some components were also "trimmed" to improve the match.

(2) Error Amplifier and AGC Control Stages

Figure III-10 shows the error amplifier and AGC control circuits. The heart of the AGC control circuit is an integrated operational amplifier which sums the output of all four peak detectors and compares this sum to a reference voltage of approximately 3 volts. If the average coutput of the peak detectors is above the reference, the output of the operational amplifier will drop in voltage. This will cause the AGC amplifier control line to drop, and the gain of all the AGC amplifiers will be reduced. If the average output of the peak detectors is below the reference level, the gain of the AGC amplifiers will be raised, and the peak detector output will become higher. The operational amplifier output is buffered to the AGC amplifier control output by means of resistor-diode-transistor network. This is because the AGC amplifier control should not

swing below +2 volts or above +11.4 volts. The operational amplifier output, however, will swing from -4.5 to +10.5 volts depending on the peak detector outputs.

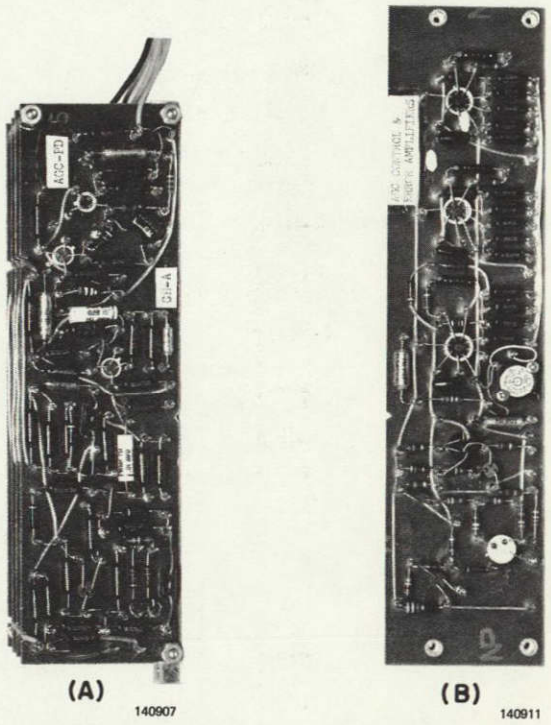

Figure III-9. (a) AGC Amplifier and Peak Detector Circuit Board and (b) AGC Control and Azimuth and Elevation Error Amplifier Circuit Board

When the receiver signal levels are so strong that the AGC amplifiers are driven to their lowest gain state, the AGC transmitter control starts to become activated. This circuitry compares the operational amplifier output to a fixed reference level and supplies a zero to 0.5 milliampere signal to the transmitter, depending on how far below the reference level the output is. This signal current is used to lower the transmitter output, which consequently lowers the receiver signal levels.

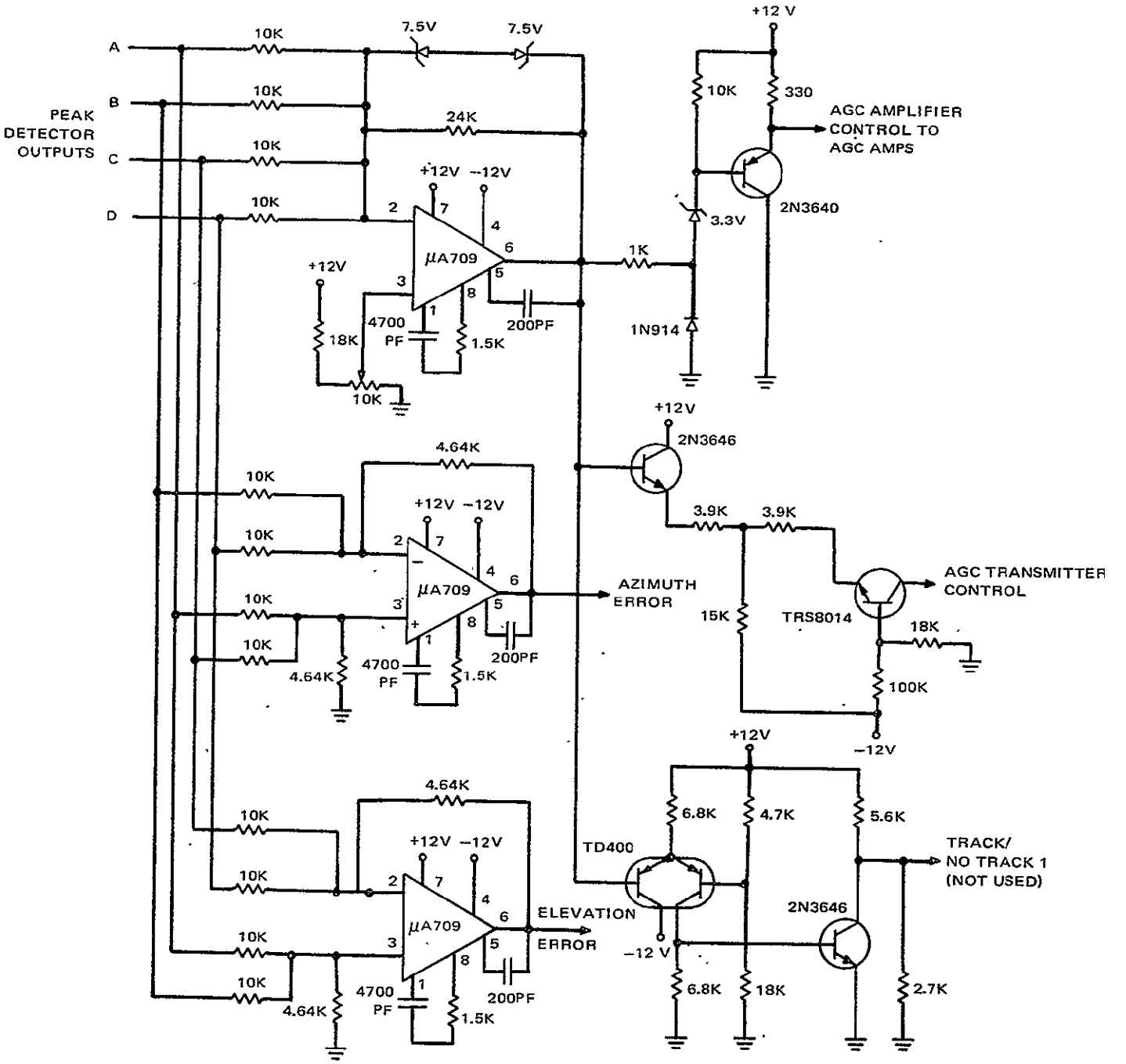

CAPACITANCE IS μF, RESISTANCE IS OHMS, UNLESS OTHERWISE SPECIFIED.

Figure III-10. Error Amplifier and AGC Control, Schematic Diagram (Schematic 3)

The operational amplifier output is connected to a second comparator circuit which triggers when the receiver is receiving signals. When the operational amplifier output drops below the reference level of this circuit, a small current will switch from one of the matched transistors to the other and the Track, No-Track line will switch to about 4 volts. This circuit, however, was not used due to lack of sensitivity at maximum range.

Azimuth and elevation errors are derived from operational amplifiers connected in a sum and difference configuration. To develop the required error function, the error outputs are derived as follows:

$$\text{Azimuth Error} = 0.464\ [\text{Peak Det A} + \text{Peak Det C} - \text{Peak Det B} - \text{Peak Det D}]$$

$$\text{Elevation Error} = 0.464\ [\text{Peak Det A} + \text{Peak Det B} - \text{Peak Det C} - \text{Peak Det D}]$$

The circuit board shown in Figure III-9(b) contains the AGC control circuits and azimuth and elevation error amplifiers.

(3) Tracking Circuitry Operation

The tracking circuitry was tested to determine what shifts in the electrical boresight of the transmitter unit would be obtained when the inputs to the AGC amplifiers varied from 3 millivolts to 3 volts and when the environmental temperature was varied from 0°C to 50°C. The results are listed in Table III-1, which also shows the laboratory test setup. Equal pulse inputs were applied to all four AGC amplifiers and the outputs of the azimuth and elevation error amplifiers were observed for deviations from zero volt. An error indication on either output of 0.7 volt corresponds to about 1 milliradian of electrical boresight shift.

The gain control capability of the tracking circuitry was tested by varying the voltage amplitude of the input pulse to the AGC amplifiers and monitoring the peak detector outputs and the transmitter and amplifier control voltages. The results of these measurements are listed in Table III-2. This data confirms that the transmitter output and AGC amplifier gain are maximum for the very low signal inputs.

As the signal input level is increased to about 1-volt peak, although the AGC amplifier gain is decreased, the transmitter control voltage still enables maximum output. Further increases in signal input level causes the AGC amplifier gain to level off at some minimum value. At the same time, the transmitter control voltage starts dropping until, at an AGC input level of about 3.8 volts, the transmitter output is reduced to zero, as indicated in Figure III-4.

TABLE III-1. EFFECT OF CHANGES IN SIGNAL AMPLITUDE AND TEMPERATURE ON ELECTRICAL BORESIGHT

Input	Output at 0°C			Output at 25°C			Output at 50°C		
	AGC	AZ	EL	AGC	AZ	EL	AGC	AZ	EL
3.0	4.42	+0.43	-0.04	3.36	+0.07	+0.09	2.32	-0.44	+0.10
1.0	8.12	+0.61	-0.06	7.13	+0.22	+0.23	6.18	-0.25	+0.22
0.3	9.20	+0.39	-0.10	8.46	+0.10	+0.26	7.54	-0.31	+0.22
0.1	9.50	+0.17	-0.08	9.30	-0.06	+0.13	8.36	-0.45	+0.07
30 mV	10.74	+0.19	-0.10	9.79	-0.07	0.00	8.91	-0.40	-0.04
10 mV	11.14	+0.01	-0.15	10.24	-0.09	-0.08	9.45	-0.30	-0.09
3 mV	11.30	0.00	-0.06	11.20	-0.09	-0.01	11.20	-0.17	+0.04

All readings are in units except where units are specified.

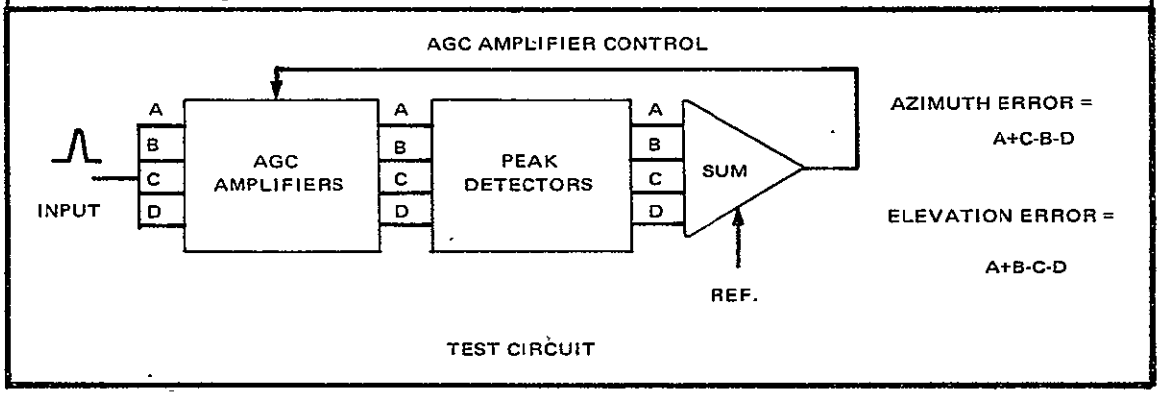

TEST CIRCUIT

TABLE III-2. AUTOMATIC GAIN CONTROL CHARACTERISTICS

Input	Amplifier Control	Xmtr Control	No. 1 Track, No-Track	Peak Detector Outputs			
				A	B	C	D
3.8	2.01	270	3.95	5.85	5.80	5.84	5.83
3.4	2.18	385	3.95	2.89	3.36	3.59	3.30
3.0	2.65	435	3.96	2.96	3.34	3.34	3.14
1.0	6.87	558	3.93	2.75	2.62	2.71	2.53
0.3	8.28	559	3.93	2.56	2.32	2.55	2.48
0.1	9.13	560	3.93	2.29	2.19	2.46	2.54
0.03	9.63	560	3.93	2.18	2.20	2.35	2.50
0.01	10.07	560	3.93	2.12	2.21	2.25	2.43
0.003	11.02	560	3.93	2.02	2.02	2.12	2.22
0.0027	11.18	560	3.93	1.79	1.77	1.86	1.93
0.0024	11.18	560	0.23	1.61	1.60	1.68	1.75

All readings are in volts.

d. Ranging Circuitry

Range is determined by measurement of the time interval between transmission and reception of the laser pulse. For accurate ranging, the counter "start" and "stop" control pulses must be generated precisely at the peaks of the transmitted and received pulses. Accuracy is enhanced by processing the derived signals through identical circuitry as much as possible.

(1) Computer Start-and-Stop Pulse Generation

The sampling diode, shown in Figure III-11 (a), detects a small portion of the transmitted light pulse which passed through the transmitter mirror (or beam-splitter) instead of being reflected towards the target. The sampling-diode preamplifier, which uses the same circuit as the receiver preamplifiers except for accommodation of the type of photodiode used, drives the start-pulse ranging circuits directly.

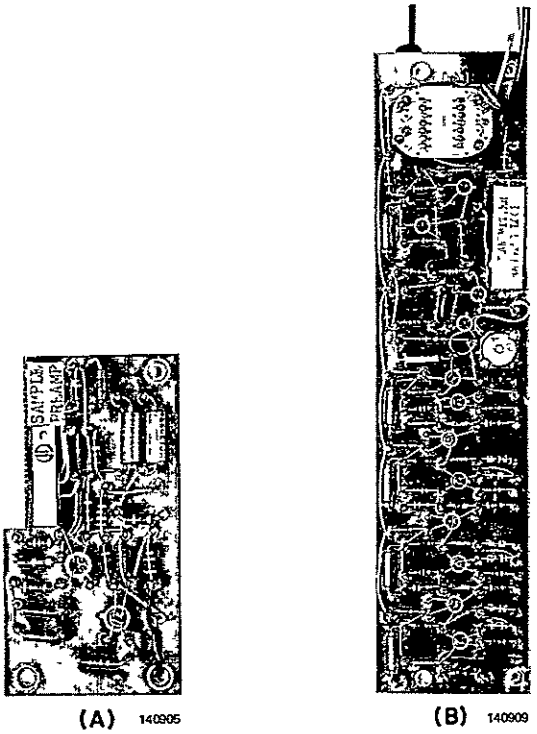

Figure III-11. (a) Sampling Diode Circuit Board and
(b) Transmitter Ranging Circuit Board

The differentiated sum signal from the receiver preamplifier is used to drive the second set of ranging circuits to derive the computer stop pulse.

The ranging circuits, a limiting amplifier, a Schmitt Trigger circuit, and a 50-nanosecond one-shot multivibrator, are shown in Figure III-11(b). Figure III-12 shows the circuit schematic for the sampling preamplifier and the ranging start and stop circuits. Note that the ranging circuits are identical, with the exception of component values at the input to the limiter circuits. This difference is necessary because there is no sum and differentiator circuit in the sampling preamplifier and differentiation must take place at the limiter input.

The limiter contains four stages of amplification, with diode limiting placed in the first three of these stages. The overall gain of the limiter is set so that the minimum anticipated input signal will produce an output which is just below the limiting level. The overall gain for the limiter circuit is about 54 dB, and the output is limited to ±2 volts. Diode limiting at the collectors of the common-emitter gain stages has been found to produce the smallest zero-crossing time shift error. Four stages of gain are used to enable the gain of each limiting stage to be kept low (12 dB). Laboratory experiments have shown that many low-gain limiting stages produce a smaller time-shift error overall than a few high-gain stages.

The Schmitt Trigger is designed to shift to its "high" state of about 4 volts when its input signal exceeds 0.8 volt. It will trigger back to zero volt when the input signal swings through zero volt. The 2000-ohm potentiometer is used to adjust the zero-crossing trigger level.

The counter one-shot multivibrator is triggered by the negative-going edge of the Schmitt Trigger output. The input transistor of this circuit is normally conducting, and the output transistor is non-conducting. When the input negative transition takes place, the input transistor is shut-off and the output transistor turns on, driving the 50-ohm load to plus 2.5 volts. The 10-kilohm resistor next charges up the 10-pF input capacitor until the input transistor begins to conduct and the output transistor is again turned off, causing the output voltage to drop to zero. The resultant output signal is a 2.5-volt, 50-nanosecond-wide pulse with a rise and fall time of 10 nanoseconds. A ranging circuit board is shown in Figure III-11(b).

(2) Accuracy Measurements

The receiver ranging circuitry for the LTRS was designed to handle a signal-input-voltage range between 3 millivolts and 3 volts with less than ±3.3 nanoseconds time shift in the detection of the peak of the signal. A test was set up in the laboratory to measure the effect of variations of input voltage and temperature on timeshifts in the ranging circuitry.

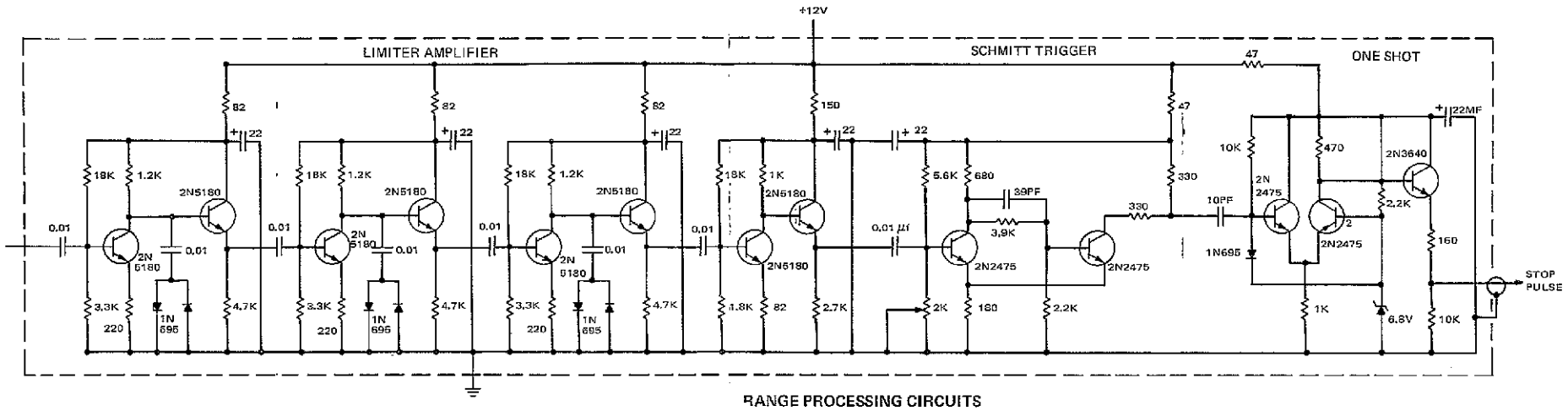

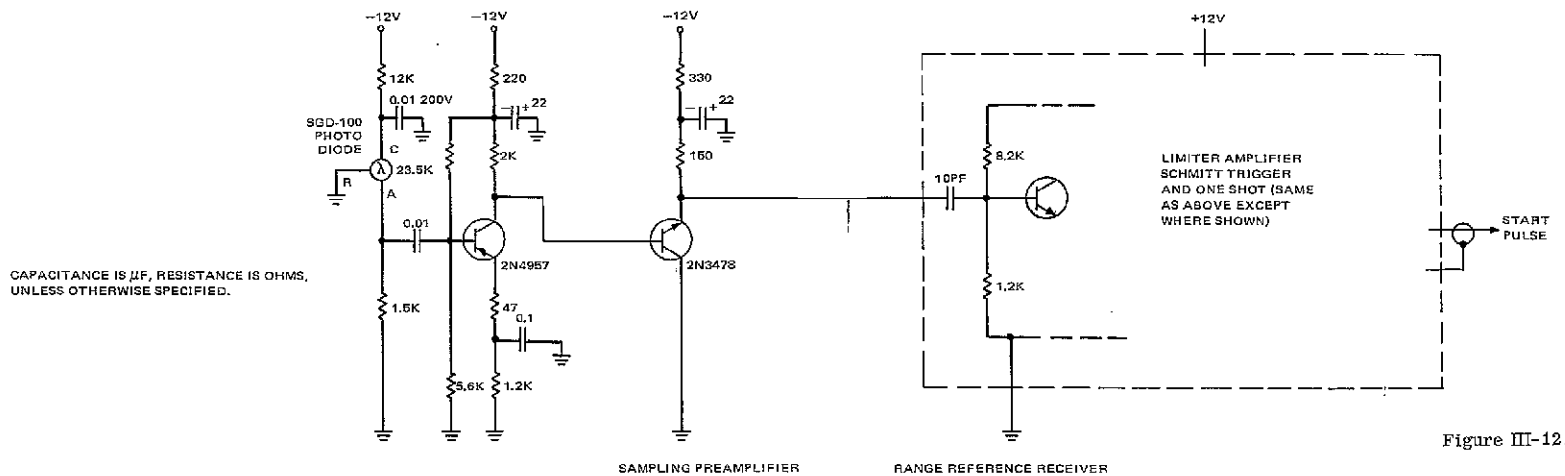

CAPACITANCE IS μF, RESISTANCE IS OHMS, UNLESS OTHERWISE SPECIFIED.

Figure III-12. Reference Receiver and Range Processing Circuits, Schematic Diagram (Schematic 4)

FOLDOUT FRAME 1

FOLDOUT FRAME 2

Figure III-13(a) shows an oscilloscope photograph of counter "stop" pulse leading edges for triangular shaped inputs of 3, 30, 300 and 3000 millivolts to the sum and differentiator circuit. In this photograph, the amplitude time-shift error is shown to be less than 2 nanoseconds.

The receiver and transmitter ranging circuits were placed in an oven and an 0.3-volt triangular pulse was applied to both inputs at the same time. Oscilloscope photographs of the leading edges of the start and stop pulses are shown in Figure III-13(b) for oven temperatures of 25°C and 50°C.

Although the start and stop pulses shift about 2 nanoseconds from 25°C to 50°C, the relative shift between the two is only about 0.5 nanosecond.

From the results of these two time-shift measurements, it can be seen that the ranging circuitry will contribute an error of only about ±0.2 meter to the range accuracy of the laser unit.

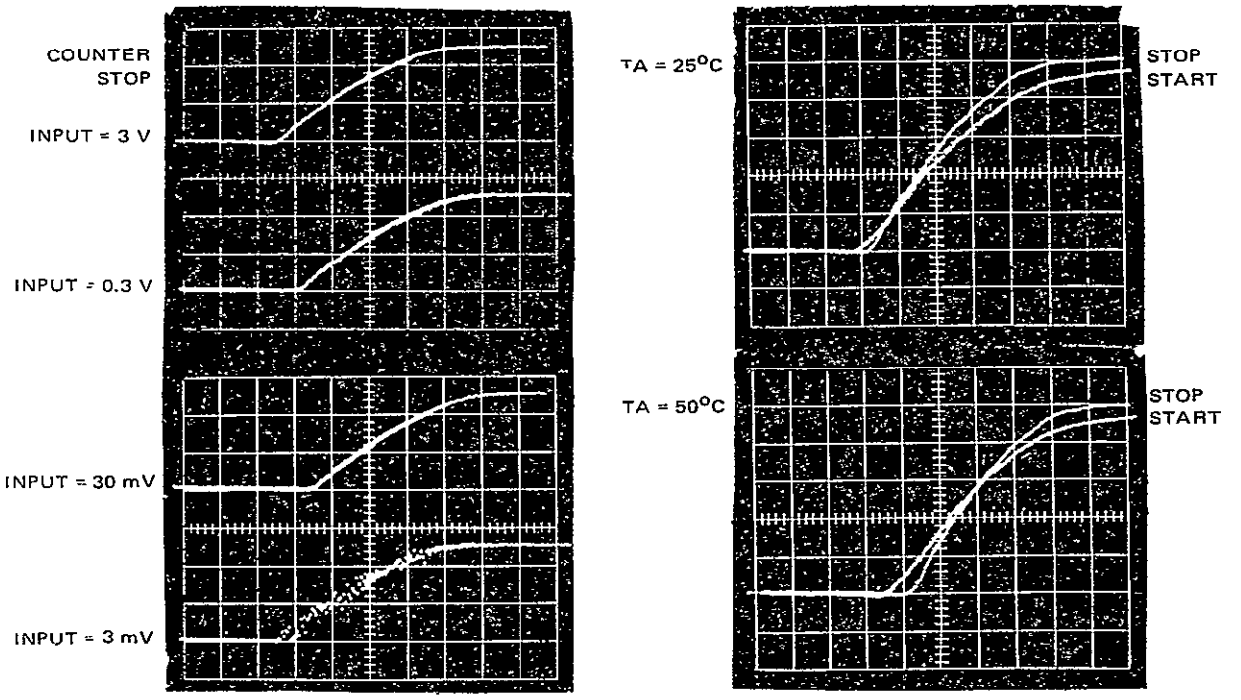

a TIME SHIFT VERSUS INPUT AMPLITUDE, VERTICAL 1V/DIV , HORIZ. 2NS/DIV.

b. TIME SHIFT VERSUS TEMPERATURE, VERTICAL 0 5V/DIV., HORIZ 2NS/DIV.

Figure III-13. Time Shifts Due to Signal Amplitude and Temperature Variations

(3) Computer-Control Logic Stages

The logic diagram for the counter control circuitry is shown in Figure III-14. Standard Signetic 8000-Series integrated circuits are used, except for the two-counter reset circuits (R1 and R2). These are one-shot multivibrators utilizing discreet components and were included because the load requirements on these signals were too severe to be handled by the integrated-circuit one-shots. The 1- and 500-microsecond one-shots (at the upper left in Figure III-14) are mounted on the receiver and transmitter ranging boards.

The counter "start" pulse triggers the 500-microsecond delay one-shot, which allows enough time for all range measurements to be completed and processed. At the end of this 500-microsecond delay period, the five-bit binary counter and a 50-microsecond delay one-shot are triggered. At the end of the 50-microsecond delay, the reset pulse R1 is generated and the R1 register of the range counter is reset. This reset pulse is a 4-microsecond, 4-volt pulse.

After 32 start pulses have been generated, the last bit of the binary counter will be triggered and another 50-microsecond one-shot will be fired. The logic "and" of the negative output from this one-shot and the "counter overflow" signal are used to provide a logic "and" with the "counter read" command to provide the "range read" signal. If the overflow signal is low (approximately zero volt) and the "counter read" signal is high (approximately 4 volts), the 50-microseconds-wide "range read" command will be generated. At the end of the 50-microsecond "range read" command, the reset pulse R2 is generated, and the output register of the range counter will be reset.

Figure III-14 also shows the logic configuration for generating the Track, No-Track command. When the start pulse triggers the 500-microsecond delay one-shot, a negative pulse is applied to the trigger input of the Track, No-Track flip-flop. Since the terminal "Rc" to the flip-flop is grounded, the negative transition of the signal applied to the trigger input will cause the flip-flop to be reset. When the counter stop pulse is generated, it triggers a one microsecond one-shot which then sets the Track, No-Track flip-flop. If a stop pulse is not generated, the flip-flop will remain reset and the Track, No-Track line will remain low, indicating a no-track condition.

e. Mechanical Components

Figure III-15 shows various views of the Laser Ranging transmitter and receiver in different stages of assembly.

The completely assembled unit is shown in Figure III-15(a). On the side of the unit can be seen the placement of the mounting supports, and the electrical

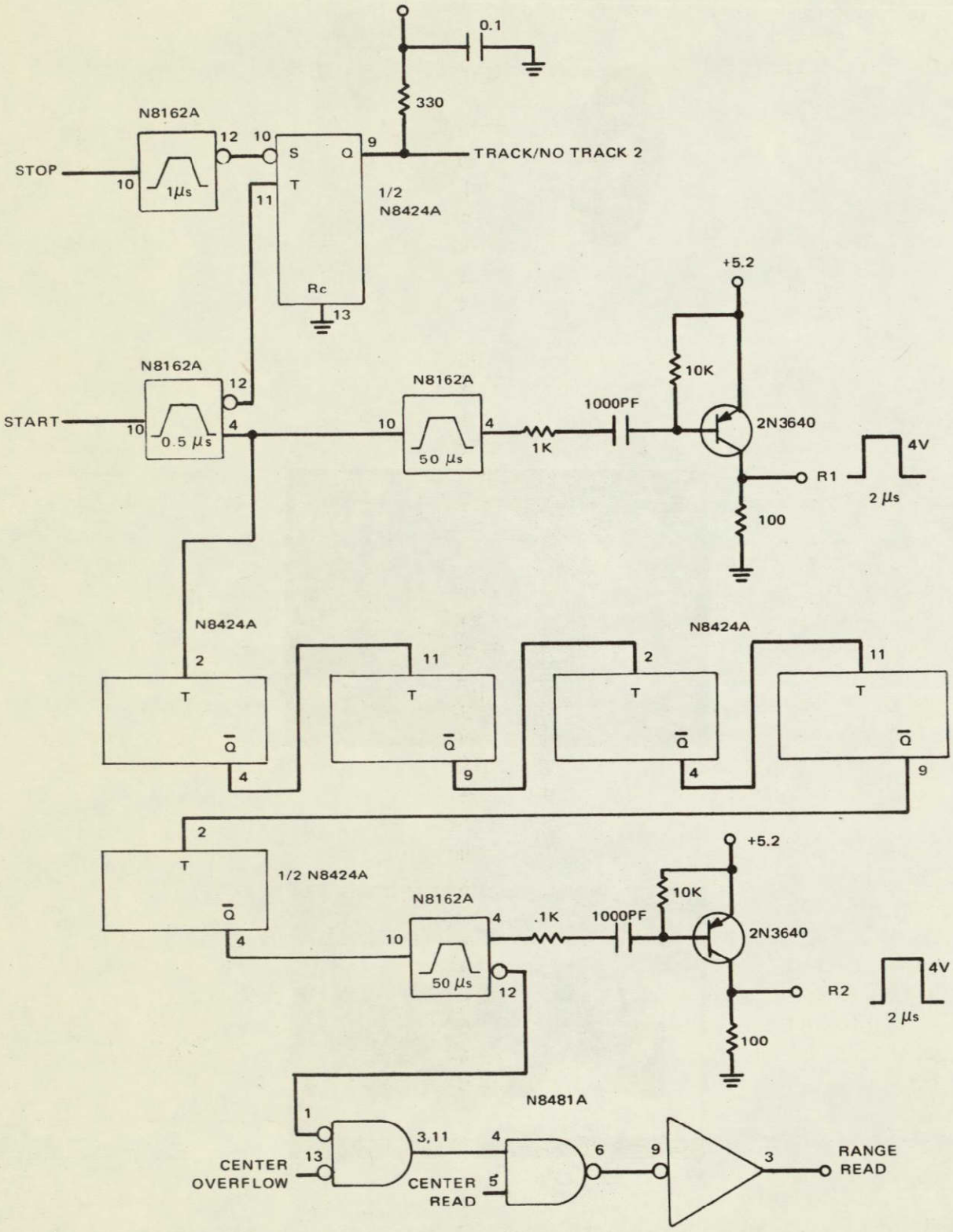

CAPACITANCE IS μF, RESISTANCE IS OHMS, UNLESS OTHERWISE SPECIFIED.

Figure 3-14. Counter Control Logic, Block Diagram (Schematic 7)

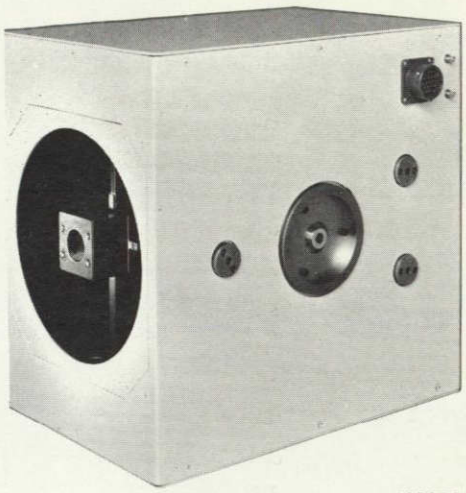

140938

(A)

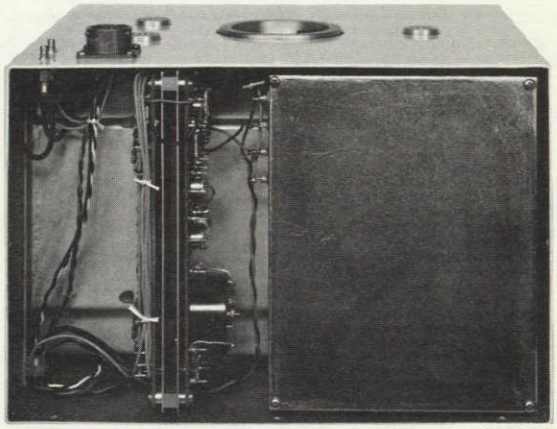

140940

(B)

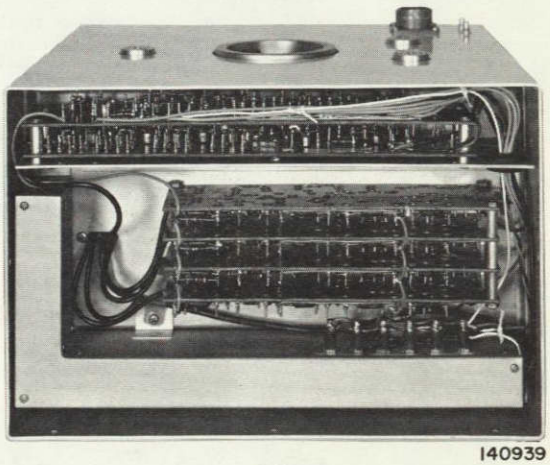

140939

(C)

Figure III-15. Laser Transmitter, (a) Completely Assembled, (b) Top Cover Removed, and (c) Bottom Cover Removed

connectors. The two subminiature coaxial connectors accommodate the counter start- and stop-pulse wiring. The 18-pin connector provides for the remaining electrical connections to the system (supply voltages, control signals, etc.). The receiver aperture and the transmitter mirror assembly mounted on the spider support, can be seen at the front. The mirror re-directs the transmitted light pulse from the laser towards the target.

A view of the transmitter-receiver unit with its top cover removed is shown in Figure III-15(b). This view shows two subassemblies mounted to the telescope tube. The mu-metal box contains the complete transmitter circuitry and the laser diode. The transmitter is housed in mu-metal to prevent excessive electromagnetic radiation from leaking into the sensitive receiver circuitry. Electrical connections to the transmitter are made by means of the four feed-through capacitors mounted on the transmitter box. The second subassembly shown in Figure III-15(b) contains the counter control logic and the dc-to-dc converter used to provide the 140-volt bias to the receiver photodiode.

A bottom view of the transmitter-receiver unit is shown in Figure III-15(c). The L-shaped box in the right-hand portion of the illustration contains the transmitter sampling loop which generates the counter-start pulse. The four AGC amplifier and peak detector boards are shown in the center of the unit. The extreme left subassembly contains the receiver ranging circuitry, the AGC control and error amplifier circuits. The receiver ranging circuits generate the counter-stop pulse, and the error amplifiers generate the azimuth and elevation error signals. The AGC control circuitry determines the proper transmitter power level and AGC amplifier gain. It also generates one of the Track, No-Track commands. The miniature cables entering from the bottom center of the picture provide the connections from the preamplifier assembly to the rest of the receiver circuits.

The preamplifier subassembly and housing are shown in Figure III-16. The spider housing fits into the telescope tube and the pre-amplifier assembly slides into this housing. The receiver quadrant photodiode can be seen mounted into one end of the preamplifier assembly; the transmitter mirror is mounted at the other end.

The telescope mirror and background filter assembly is shown in Figure III-17. This assembly mounts into the back of the telescope tube. The mirror is a 5.5-inch polished aluminum dish. The background filter has a 200 Angstrom pass band centered at 9200 Angstroms; it prevents excessive background light noise from being picked up by the receiver photodiode. (A Plexiglass mock-up is shown in place of the actual filter, which was not available for the illustration.)

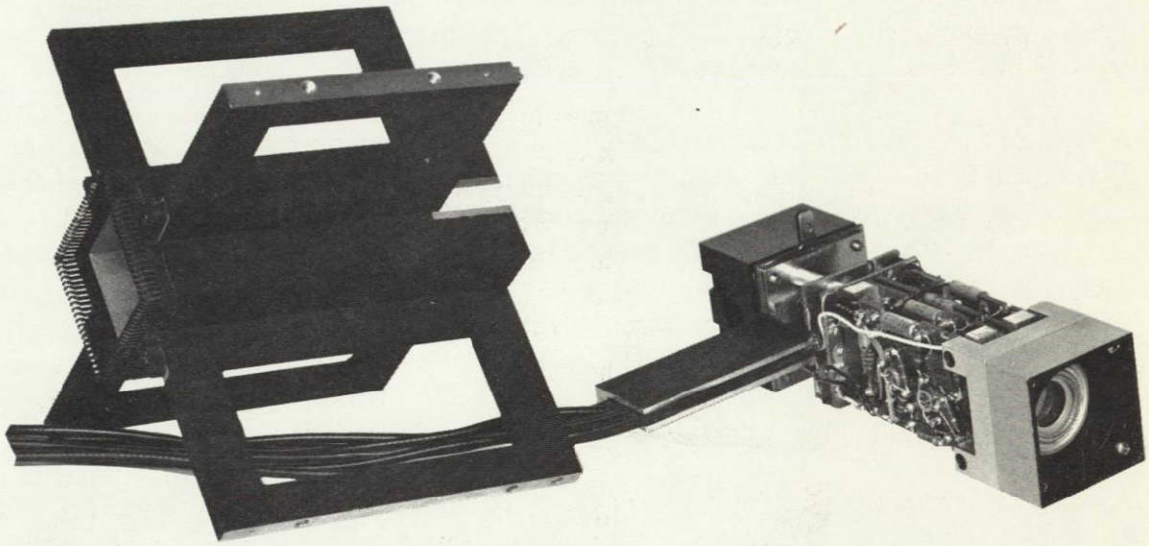

140525

Figure III-16. Preamplifier Subassembly and Housing

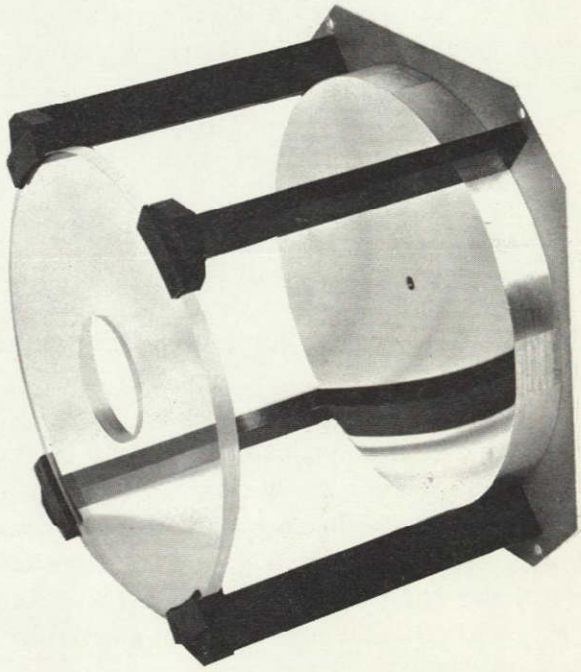

141488

Figure III-17. Telescope Mirror and Background Filter Assembly

SECTION IV. TRACKING PEDESTAL SUBSYSTEM

A. PEDESTAL COMPONENTS

The tracking pedestal was designed to mount and aim the laser unit and the boresighted TV camera. The azimuth and elevation axes are servo-driven by error signals derived in the receiver, so that the transmitter, receiver, and camera are continuously directed toward the retroreflector target. Optical shaft encoders on each axis provide continuous digital readout of azimuth and elevation angles to an accuracy of 13 bits (that is, one part in $2\pi/2^{13}$ radians).

The tracking pedestal subsystem is shown in Figure IV-1. A dummy camera and sighting telescope is mounted at the structural location designed for the operational Government-furnished equipment.

The tracking pedestal base has a standard threaded adapter for mounting to a K&E optical stand. The base also has provision for interconnections to the rack-mounted equipment, connecting cables for the range computer, and provision for a TV camera connector.

The tracking pedestal is connected to the mounting base through a ball joint and is held in position by four leveling screws. The ball joint and interconnecting cables are maintained dust-free by enclosure in a plastic bellows.

The azimuth-drive unit and azimuth encoder are contained within the cylindrical assembly above the leveling plate. This assembly has an annular construction, with all electrical cabling running up the open center. This construction provides the required azimuth freedom without the need for slip rings.

The azimuth axis has a mechanical travel of ±185 degrees, with urethane-faced shock isolators at the limits. Electrical drive limit switches are actuated at ±180 degrees of travel. The electrical and mechanical limiting devices are located externally just under the azimuth turntable. The azimuth axis uses a single, four-point contact, ball bearing, which is permanently lubricated and sealed with a teflon ring with a garter spring. A lock pin is provided to fix the azimuth axis during handling and setup of the tracking pedestal. Two bubble-levels are provided for accurate leveling of the instrument.

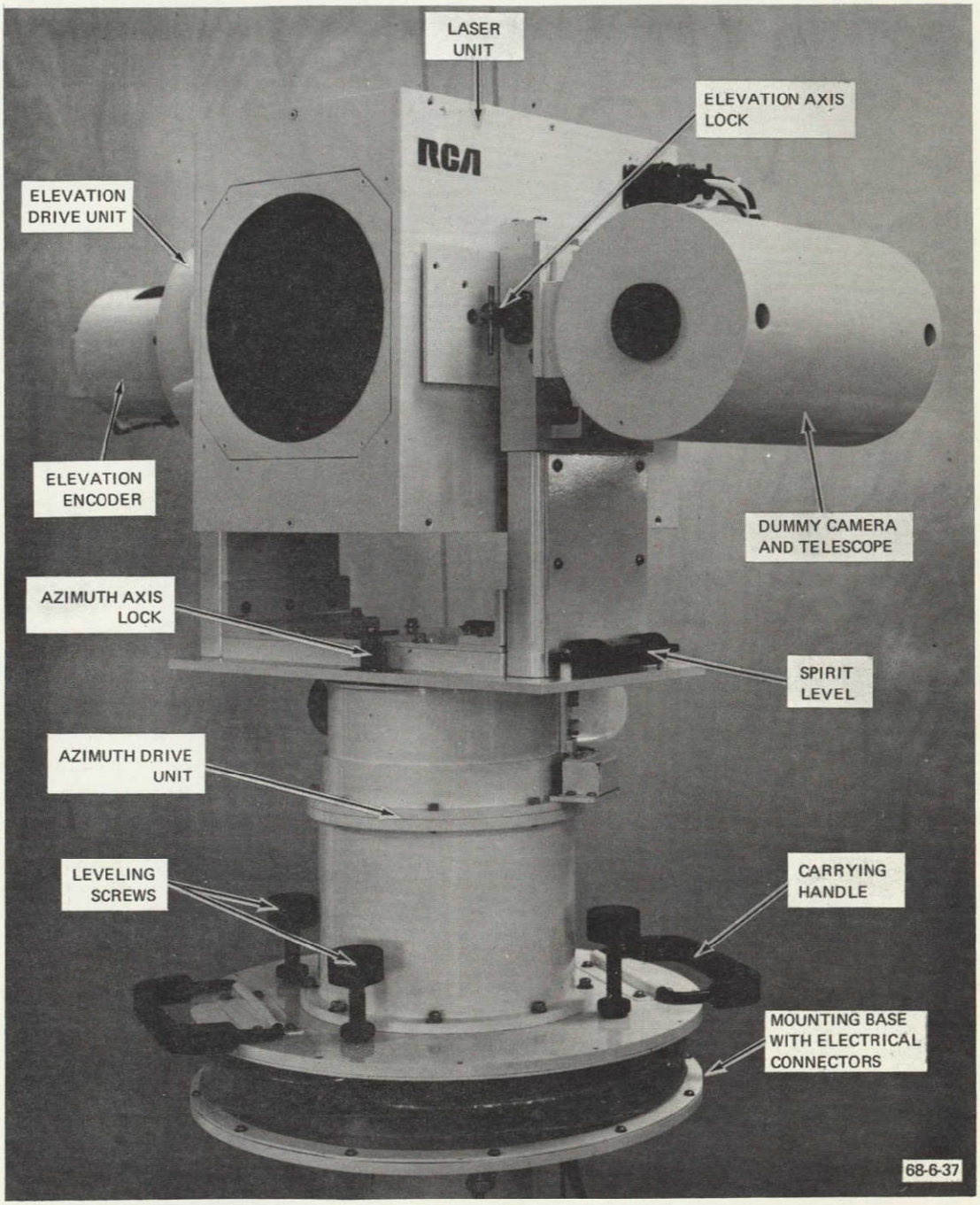

Figure IV-1. Laser Ranging and Tracking Unit, Identification of Pedestal Equipment

The elevation axis has a mechanical travel of +90 degrees to -50 degrees, also limited by shock isolators. The 90-degree positive position allows access to the tracking receiver, which is located on the underside of the transmitter-receiver unit. Electrical limit switches are actuated at ±45 degrees, which inhibits electrical drive beyond these points. Freedom in elevation is provided by two bearings supported by a yoke assembly, which is mounted to the azimuth axis. Four-point contact bearings are used, also, and are sealed in the same manner as in the azimuth axis. The elevation encoder and drive unit are located on one side of the yoke. Thus the transmitter-receiver and camera assembly are free to move, or be driven, in both azimuth and elevation axes. A lock is provided on the elevation axis to hold the assembly in position during setup.

Both elevation and azimuth drive units use direct-drive torque motors and dc tachometers manufactured by Inland Motors, Inc., and 13-bit optical shaft encoders manufactured by the Wayne-George Co.

All structural elements are fabricated from aluminum alloy. All outside surfaces are painted with a glossy white enamel having a low absorptivity-to-emissivity ratio to minimize heating from sunlight.

All structural elements are fabricated from aluminum alloy. All outside surfaces are painted with a glossy white enamel having a low absorptivity-to-emissivity ratio to minimize heating from sunlight.

B. SERVO SYSTEM DESIGN

The design of the pedestal servos is based upon (1) the system requirements of a dynamic target-following error of less than 0.5 degree when tracking a target at 20 degrees per second and (2) a capability of acquisition and lock-on to a stationary target from a 10 degrees per second scanning velocity. This latter requirement establishes the servo motor sizing and power consumption. The azimuth axis will be described here since it has greater inertia and a smaller beamwidth and, thus, provides the most difficult requirements.

1. Lock-on. The size of the azimuth motor was established on the basis of the torque needed to stop the azimuth axis inertia within 0.5 degree upon receipt of a lock-on signal. The lock-on signal is obtained from the ranging circuitry and has a time constant of less than 20 milliseconds associated with it. The angular stopping distance is determined by the pedestal angular momentum and the motor and friction torques available for stopping the pedestal.

2. Inertia. Since azimuth inertia affects stopping distance directly, the pedestal was designed for minimum inertia. The original RCA proposal to the Manned Spacecraft Center presented a mechanical configuration wherein the azimuth axis was a column which supported an elevation drive unit directly above,

with the camera and transmitter-receiver unit mounted outboard to either side of the drive unit. The azimuth inertia for this configuration was at least 5 in-lb/sec^2. It was reduced to 3 in-lb/sec^2 by changing to a yoke design in elevation where the greatest inertia member (the transmitter-receiver) is mounted directly over the azimuth axis.

3. Motor Selection. The Inland Model T4424 torque motor was chosen for its high torque, good torque-to-weight ratio, and its favorable diameter. Before friction and inertia levels were well established, it was decided that one motor should be used in elevation and one in azimuth, but with provision for an additional motor in azimuth if required. (On a weight basis, two T4424's in azimuth are better than a single motor with equivalent torque output.) The azimuth power amplifier was chosen to provide the power reserve. Subsequent estimates of inertia and friction indicated that only one motor was required.

4. Tachometer Loop. The following factors were considered in design. High gain is desirable (1) for saturation of the power amplifier, resulting in maximum torque for lock-on, and (2) for high torque sensitivity, to minimize static error due to friction and wind torques. Tachometer loop gain is limited by (1) the effect of the pedestal resonant frequencies, (2) the tachometer ripple voltage at maximum tracking rate, and (3) the laser receiver noise level.

The Inland Motors TG-4401-B tachometer is dimensionally compatible with the torque motor and has the highest gain of any standard winding. The spatial ripple frequency is 71 cycles per revolution. At 20 degrees per second, this turns out to be 4 Hz. At lower tracking rates this frequency is proportionally lower. It was not feasible to realize any significant reduction in ripple by filtering. The design value for the tachometer loop gain, therefore, was established at 427, which is just below the value that would cause saturation of the power amplifier from the ripple.

5. Tracking Loop. The azimuth tracking loop employs typical lag-lead compensation for stabilization. The bandwidth of the system is low, consistent with the target dynamics. It is assumed that lock-on occurs with the target essentially at standstill. When tracking an astronaut in motion, the response of the pedestal may directly affect the quality of the TV image. If the astronaut carrying the retroreflector moves erratically or in short jerky motions, fast servo response might cause a blurred image. Furthermore, a wide bandwidth would cause greater noise perturbation of the axis with the target stationary and at maximum range, when high accuracy is desired. Near maximum range where noise is most significant, low bandwidth also aids in maintaining lock-on. These operational reasons for using a narrow bandwidth are reinforced by power and weight considerations. If the structural resonant frequency in either axis is to be a decade above the loop cross-over frequency, it is clear that increasing the crossover frequency results in increasing the minimum structural resonance

by the same ratio. For a given structural configuration, this is reflected in greater weight. For an increased weight, increased power is also required to maintain the same lock-on performance. Therefore, to arrive at a lightweight, smooth-tracking pedestal design for flight use, the bandwidth is kept as low as possible, consistent with the maximum target dynamics.

6. Servo Operation. The schematic diagram for the azimuth and elevation servos is shown in Figure IV-2. The only differences between the two servos are that the azimuth axis has a scan velocity input for acquisition scanning and the azimuth power amplifier has a higher drive capability than the elevation power amplifier.

For each axis, the tracking servo signal is amplified in a compensation amplifier and the output is supplied to the power amplifier. The compensation amplifier gain establishes the dynamic following error of 0.5 degree for 20 degrees per second and provides balance and gain controls.

The output of the compensation amplifier is routed through the Track, No-Track relay and the slew control relay to the power amplifier. The power amplifier drives the torque motor for that axis. Velocity feedback is provided around the power amplifier by a dc-tachometer whose output is applied to the input of the power amplifier.

When the Track, No-Track or slew control relay opens the tracking loop, the velocity loop acts as a speed-control servo for acquisition scanning or slew control. When the tracking loop is closed, the system acts as a position servo stabilized by velocity feedback.

C. TRACKING AND ACQUISITION

The azimuth and elevation servos and acquisition logic are designed to provide the required target tracking and acquisition scanning when the target track is lost. There are four basic modes of operation of tracking pedestal which may be described as follows:

1. Scanning Modes

a. Normal Track and Acquisition Mode. This is the primary mode used for tracking and re-acquiring a lost target. The target is tracked within azimuth and elevation limits if the received signal is above threshold. If the target is lost, the azimuth and elevation axes are stopped at the point of target loss. After a 10-second interval, if the target has not been re-acquired, an azimuth scan is begun where the pedestal swings 11-1/4 degrees to one side, 22-1/2 degrees to the other side, and so on, providing ever increasing limits to the scan. When the target is re-acquired, normal tracking resumes.

b. Limit Scan Mode. If an azimuth electrical limit is sensed during acquisition scanning, the scanning mode changes to one where the pedestal scans between the electrical limits until the target is re-acquired. This limit scan mode is also entered if an electrical limit is sensed during tracking and the target is subsequently lost. This allows the system to follow a target through the azimuth limits. There is no time delay before this scan begins.

c. Acquisition Scan Disable. A control is provided that disables the acquisition scan mode. With the scan disabled, if the target is lost, the tracker remains indefinitely at the position it had when the target was lost. However, if track is lost beyond an electrical limit, the limit scan mode, which is not disabled, is entered, allowing the LTRS to "track through" the azimuth limit.

d. Manual Remote Positioning. The pedestal may be manually positioned by the actuation of a slew control and operation of a two-axis joy stick, which is used to insert small, variable velocities into the azimuth and elevation axes. The slew control overrides both the tracking and scanning mode so that the pedestal may be positioned manually at any time. When the slew control is released, tracking resumes if the target is within the receiver field of view; otherwise, acquisition scanning starts after a 10-second delay.

2. Acquisition Control Logic

The acquisition control logic provides the control for both the scan modes and slew control. In describing the acquisition logic, reference is made to the card and logic element numbers (for example: A12-3 is card 12, element 3) shown in the logic diagram in Figure IV-3.

Control of the acquisition scan pattern is determined by the Track, No-Track signal from the receiver. With a "track" condition, all the logic is held in a reset state through gates A22-1 and A21-1, and by reset drivers A27-1 and A27-2. Lamp and relay drivers A12-3, A12-4, and A12-7 are active, holding the azimuth and elevation tracking loops closed and illuminating the track lamp.

When a "no-track" indication is received, the reset condition is terminated and two one-shot multivibrators, A24-1 and A24-2, are triggered in sequence, providing a time delay of 12 seconds. At the end of this time, the scan control flip-flop, A27-3, is triggered, activating the scan control relay and gating the output of the azimuth encoder channel 5 into the divide-by-eight counter of A201. Channel 5 provides triggering transitions every 1.4 degree of azimuth rotation. The output of the divide-by-eight counter cycles every 11-1/4 degree, which is the basic increment of the scan pattern.

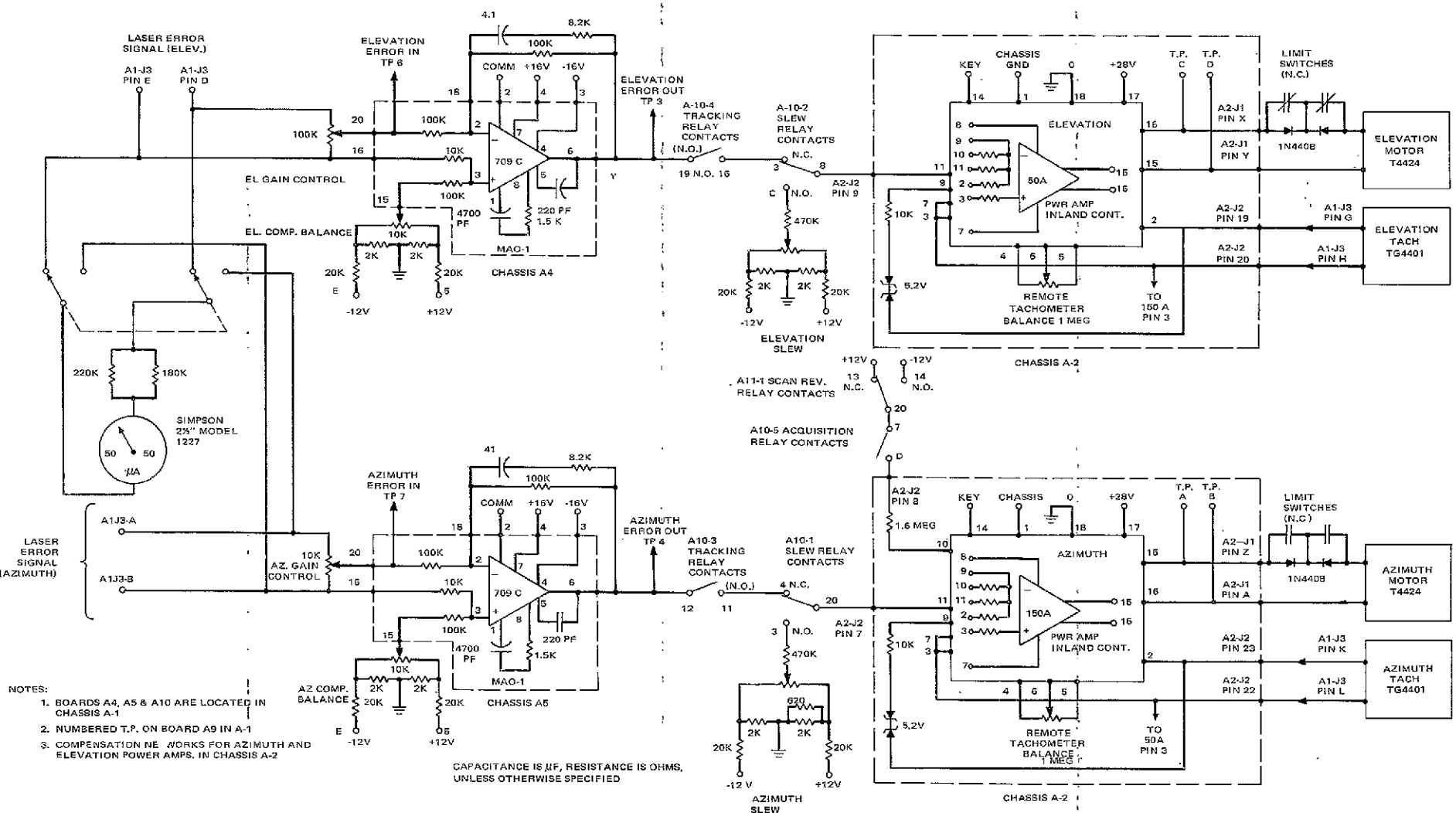

Figure IV-2. Servo Control Circuits, Schematic, Block Diagram (Schematic 8)

FOLDOUT FRAME

FOLDOUT FRAME 2

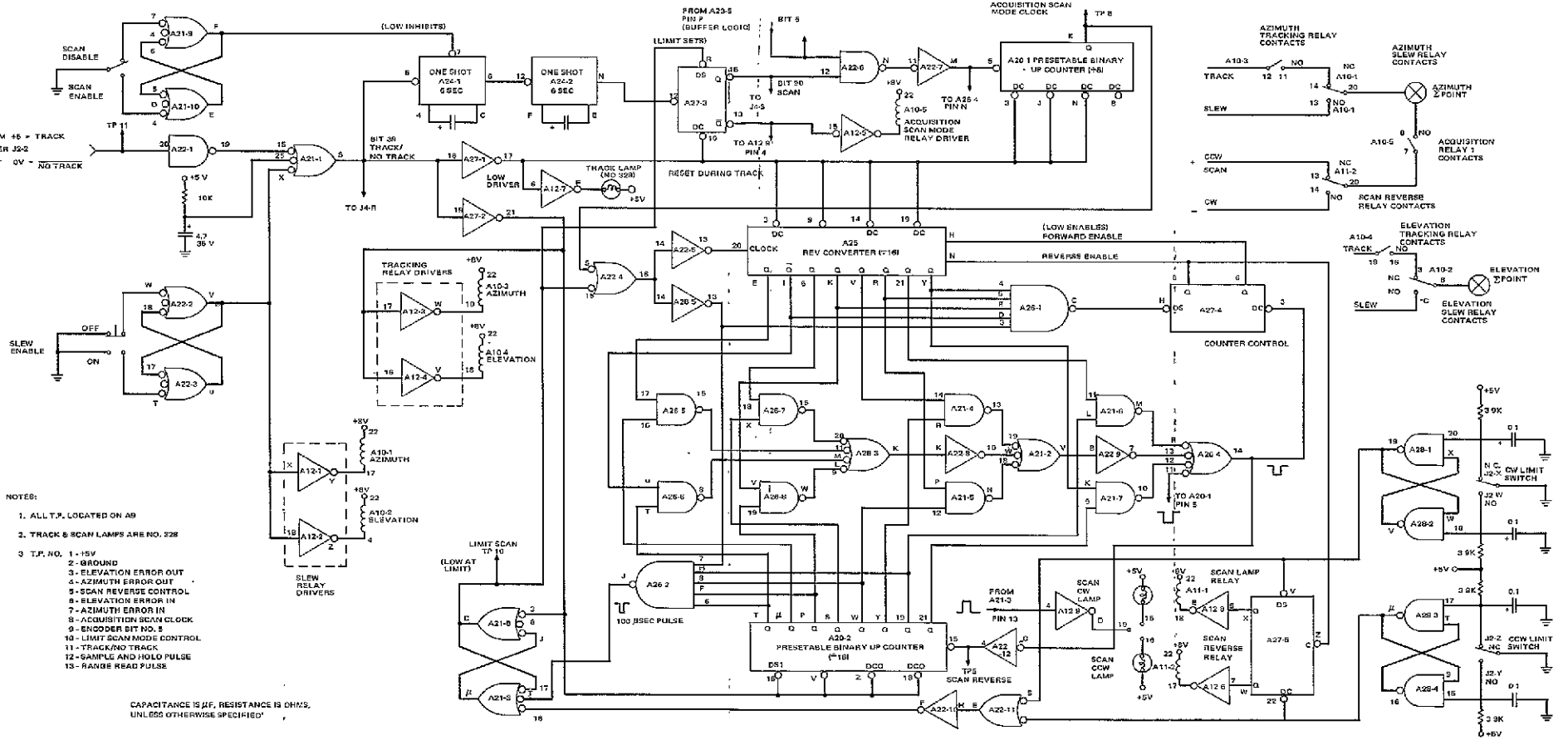

Figure IV-3. Acquisition, Logic Diagram (Schematic 9)

FOLDOUT FRAME 1

FOLDOUT FRAME 2

The reversible counter, A25, counts the number of 11-1/4 degree increments. It initially counts up (forward) until its content matches the content of the scan limit counter, A20-2, which is a presentable binary counter. This comparison is made by the array of gates in A21 and A26 which end with the comparison decision at the output of A26-4. When the content of the two counts is identical, the counter direction control flip-flop, A27-4, is reset to reverse the A25 counter.

The A25 counter continues to count in a reverse direction until its content is zero, as sensed by A26-1. At this point, the A27-4 flip-flop is set and the counter is controlled to count forward again.

The scan direction is controlled by flip-flop A27-5 and is triggered every time a scan limit is sensed by A26-4. Also, the scan-limit counter is incremented after each comparison From A26-4.

Table IV-1 illustrates the sequence of the acquisition scanning to clarify the relationships of the events described above.

The limit-scan mode is controlled by the azimuth limit switches that directly set the scan control flip-flop, A27-5 through latching circuits made up of A28-1, -2, -3, and -4. They also set the latching circuit made up of A21-3 and A21-8 which inhibits the clock input to the normal limit logic and directly set the scan control flip-flop, A27-3, bypassing the 12-second delay of the tandem one-shot multivibrators.

The slew mode is controlled by the "slew enable" button, which, through the latching circuit made up of A22-2, and A22-3, produces a track indication and actuates relays which connect the servo power amplifier to the slew velocity control instead of the outputs of the compensation amplifiers.

3. Data Buffer Logic

The data buffer logic, shown in Figure IV-4, provides a temporary store of azimuth, elevation, and range data to be sampled by an external data subsystem. Upon receipt of a "sample and hold" signal, azimuth and elevation data are transferred from the encoders into the first 25-bit positions of the buffer. Range data, which are computed continually, are transferred into bit positions 26 to 37 as soon as they are computed. However, the sample-and-hold signal inhibits the transfer to prevent erroneous range data if sampling were to take place during a range data transfer. Bit position 38 is a status indicator, showing whether or not the range data have been updated since the preceeding sample-and-hold pulse. Two other status indicators are made available to the external data subsystem from the acquisition logic. Bit 39 indicates Track, No-Track; Bit 40 indicates acquisition scanning.

TABLE IV-1. SEQUENCE OF ACQUISITION SCANNING

Clock Pulse Number to A25 Counter	Content of A25 Counter	Content of Scan Limit Counter (A20-2)	Scan Direction	Azimuth Deviation from Initial Point at Time of Scan Reversal	Remarks
initial condition	0	1	+	0°	Scan begins
1	1	2	-	+11-1/4°	First scan reversal, A25 reversed, A20-2 incremented
2	0	2	-		A25 forward
3	1	2	-		
4	2	3	+	-22-1/2°	Second scan reversal, A25 reversed, A20-2 incremented
5	1	3	+		
6	0	3	+		A25 forward
7	1	3	+		
8	2	3	+		
9	3	4	-	+33-3/4°	Third scan reversal, A25 reversed, A20-2 incremented
10	2	4	-		

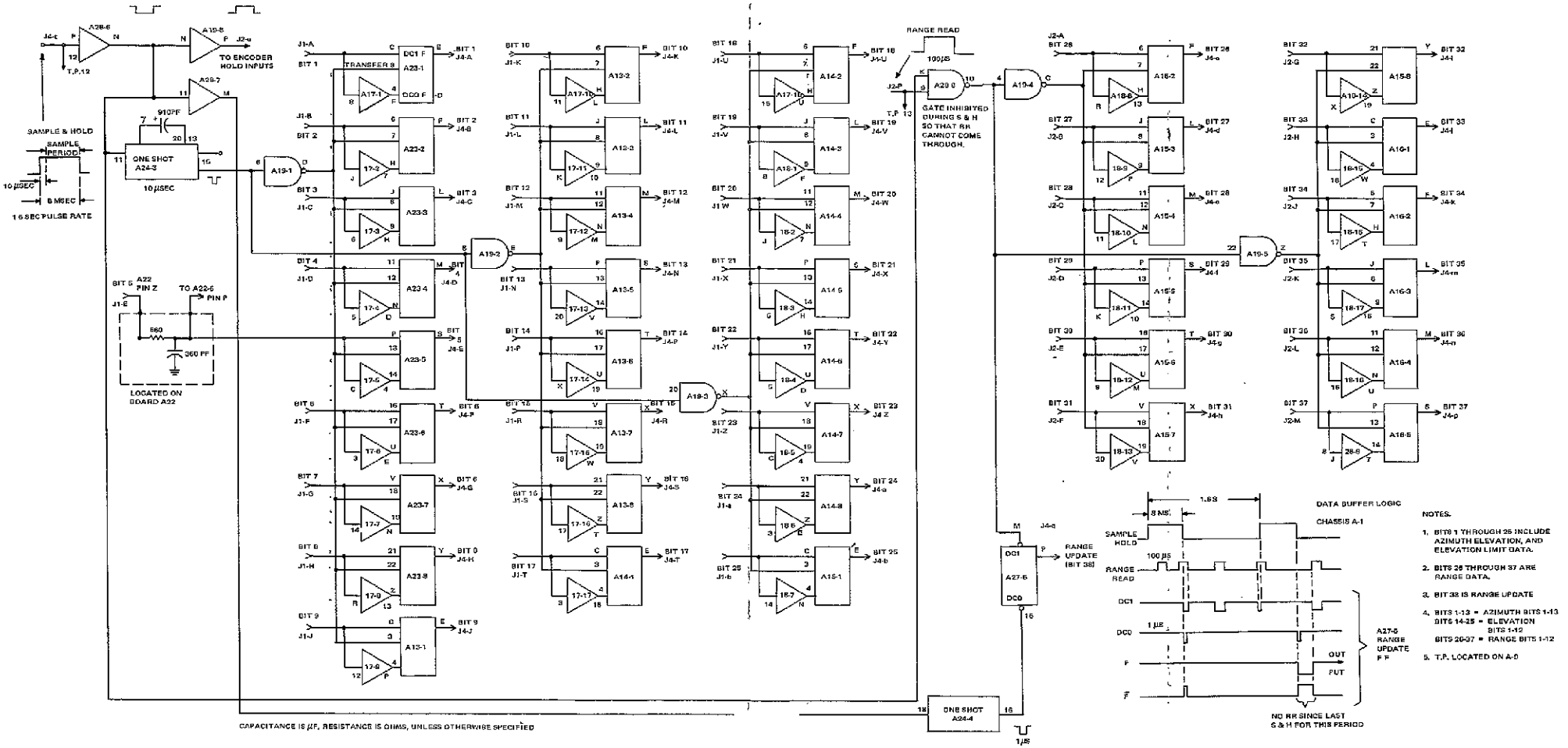

Figure IV-4. Output Data Buffer, Logic Diagram (Schematic 10)

Table IV-2 given and defines the data output to the external data system. For any data output line, a binary "1" is indicated by a 4 ±1 volt level; a zero, by a 0 ±0.5 volt level.

TABLE IV-2. DATA OUTPUT DEFINITION

(Connector pin numbers refer to J5 on control unit chassis)

Bit Position	Description	Translation	Connector Pin No.
1	Azimuth Bit #1	*0.04°	A
2	Azimuth Bit #2	*0.09°	B
3	Azimuth Bit #3	*0.18°	C
4	Azimuth Bit #4	*0.35°	D
5	Azimuth Bit #5	*0.70°	E
6	Azimuth Bit #6	*1.41°	F
7	Azimuth Bit #7	*2.81°	G
8	Azimuth Bit #8	*5.63°	H
9	Azimuth Bit #9	*11.25°	J
10	Azimuth Bit #10	*22.50°	K
11	Azimuth Bit #11	*45.00°	L
12	Azimuth Bit #12	*90.00°	M
13	Azimuth Bit #13	*180.00°	N
14	Elevation Bit #1	*0.04°	P
15	Elevation Bit #2	*0.09°	R
16	Elevation Bit #3	*0.18°	S
17	Elevation Bit #4	*0.35°	T
18	Elevation Bit #5	*0.70°	U
19	Elevation Bit #6	*1.41°	V
20	Elevation Bit #7	*2.81°	W
21	Elevation Bit #8	*5.63°	X
22	Elevation Bit #9	*11.25°	Y
23	Elevation Bit #10	*22.50°	Z

* These values represent binary weight.

TABLE IV-2. DATA OUTPUT DEFINITION (Continued)

(Connector pin numbers refer to J5 on control unit chassis)			
Bit Position	Description	Translation	Connector Pin No.
24	Elevation Bit #11	*"1" = 0.00° "0" = -45.00°	A
25	Elevation Limit	"1" = Beyond ±45°, "0" = in limits	B
26	Range Bit #1	0.5 Meters	C
27	Range Bit #2	1.0 Meters	D
28	Range Bit #3	2.0 Meters	E
29	Range Bit #4	4.0 Meters	F
30	Range Bit #5	8.0 Meters	G
31	Range Bit #6	16.0 Meters	H
32	Range Bit #7	32.0 Meters	I
33	Range Bit #8	64.0 Meters	J
34	Range Bit #9	128.0 Meters	K
35	Range Bit #10	256.0 Meters	M
36	Range Bit #11	512.0 Meters	N
37	Range Bit #12	1024.0 Meters	P
38	Range Update	"1" = Update since S and H, "0" = no update	Q
39	Track/No-Track	"1" = Track, "0" = No-Track	R
40	Acquisition Scan	"1" = Scan, "0" = No scan	S
	Sample & Hold	----------	T
	Data Common	----------	U

* These values represent binary weight.

SECTION V. SYSTEM AND SUBSYSTEM TESTS

This section describes the tests performed at the subsystem and system level. Also described are the problems that arose during testing and the way in which they were solved.

A. LASER/RANGING SUBSYSTEM TESTS

The complete Laser/Ranging Subsystem performed well during initial tests. However, some modifications were made as a result of field testing. During these tests, it was discovered that the received signal power levels at maximum range were not as large as had been anticipated. To compensate, the gain of the preamplifier was increased from 20 to 26 dB.

The optical filter used to reduce the background light incident on the photodiode was originally a 1-inch diameter interference filter placed on the face of the photodiode. This configuration was abandoned because the incident signal was not collimated at this point, and excessive attenuation of the received signal resulted. An interference-type filter then was placed in line with the telescope receiving mirror, as shown in Figure III-17.

The Laser/Ranging Subsystem was tested under various atmospheric conditions. A cloudy or hazy day had a definitely detrimental effect on the range capability of the system. Under clear nighttime conditions, operation was sustained to a range of about 840 meters without the receiver optical filter. Under all of these conditions, the range and error positioning accuracies were within ±1 meter and ±0.04 degree, respectively.

B. TRACKING PEDESTAL SUBSYSTEM TESTS

Some preliminary tests were performed on the azimuth and elevation servos before assembly of the complete subsystem. The remainder were performed with the complete subsystem.

One problem became apparent during the testing of the drive units, which are sealed against dust and other contaminants by a spring-loaded teflon ring which slides along aluminum surfaces. It was found that the teflon was causing the removal of some aluminum in the form of a blackish powder. To eliminate this, the drive units were disassembled, and the aluminum surfaces were plated with nickel under chromium.

The assembled drive units were tested and the torquers and tachometers were found to operate satisfactorily. However, excessive electrical coupling existed between the torquers and tachometers in spite of the shielding incorporated between the two units, causing unstable operation of the velocity control loop when operated at the design value for open-loop gain. A temporary fix was made by reducing the gain and filtering. Later, with the subsystem fully assembled and operating, open- and closed-loop-response from 1 to 800 Hz was measured and a filter was designed for compensating the velocity loop for stable operation. Also, the amplifier gain in the velocity loop was reduced from 427 to 200.

C. SYSTEM PERFORMANCE TESTS

For system performance testing, an accurately surveyed range was set up. Markers were placed along an established baseline at ranges of 12, 30, 80, 250, 300, 500, and 700 meters from the instrument station. Elevations were taken at each marker station so that a level sight could be established along the baseline to any of the seven range markers.

The system performance testing primarily covered the measurement of ranging accuracy to each range marker and the measurement of boresight accuracy in the azimuth and elevation axes. Azimuth accuracy tests were made relative to the baseline azimuth established by tracking a target over the 80-meter station. Elevation accuracy tests were absolute, based upon accurate leveling of the tracking pedestal.

Since the system has no provision for visual readout of azimuth, elevation, and range data, a Hewlett-Packard printer was used with a special adapter box to print out data from the buffer registers.

The acceptance plan for system performance was primarily a test for maximum range, ranging accuracy, boresight accuracy, and target re-acquisition. These tests were performed both before and after temperature and vibration testing of the tracking pedestal. The first tests were conducted satisfactorily except for the test at the 700-meter range, which could not be run because of fog. Since poor visibility was predicted for a number of days, the environmental testing was begun without completing the 700-meter test. The second series of tests were complete, however. Tables V-1 and V-2 summarize the test data taken during the initial and post-environmental performance acceptance tests.

The environmental test plan called for temperature and vibration testing of the non-operating tracking pedestal. Temperature tests were to be two 1-hour soaks: one at 40°F, the other, at 110°F. Vibration testing was to be carried out with the tracking pedestal in its carrying case, strapped to a Calidyne Model C-210 shaker. Three vibration runs were called for along the three axes. Each run was a 7.5 minute sinusoidal sweep from 8 to 500 Hz at an input level of 2.5 g peak.

TABLE V-1. FIRST PERFORMANCE TEST DATA

Range Marker Location (Meters)	Laser Measurements		
	Range (Meters)	Azimuth Deviation (Degrees)	Elevation Deviation (Degrees)
12	11.0	-0.09	+0.04
30	29.0	+0.04	+0.04
80	80.0	0.00	+0.04
300	300.0	-0.04	-0.13*
500	500.5	0.00	-0.04
700	†	†	†

*Inaccurate, due to error in elevation survey for this station.
†Not measured because of poor visibility.

TABLE V-2. FINAL SYSTEM PERFORMANCE TEST DATA

Range Marker Location (Meters)		Laser Measurements	
	Range (Meters)	Azimuth Deviation (Degrees)	Elevation Deviation (Degrees)
12	11.5	0.00	0.18
30	30.0	+0.04	+0.09
80	80.0	0.00	+0.04
300	300.5-301.0	0.00	-0.09*
500	501.0	0.00	0.00
700	701.0	-0.04	+0.04

*Inaccurate, due to error in elevation survey for this station.

Temperature testing was carried out with the tracking pedestal in a Tenney chamber. Thermocouples were attached at three points on the pedestal and thermal soaks were carried out at each temperature long enough so that the pedestal temperature stabilized at the test level for a 1-hour period. No detrimental effects were observed from temperature testing of the tracking pedestal.

Vibration testing was done in accordance with the plan after a preliminary vibration run was performed at a level of 1.0 g peak to check the amplification of the tracking pedestal response relative to the input. Peak amplifications ranged from about 2.0 to 3.0, giving peak vibration levels of 5 to 7.5 g.

Tracking pedestal vibration levels were monitored by a 3-axis accelerometer affixed inside the pedestal base adapter for the optical stand. A curve of the vibration level along the azimuth axis with the vibration being applied along the same axis is shown in Figure V-1.

After the vibration test, the LTRS was set up for system testing. It was found that tracking error signals were not being generated, and the trouble was traced to a fractured +12-volt supply lead which linked two circuit boards. There had been insufficient dress on the lead and it fractured at both ends and fell off during vibration, removing power from the Error Amplifiers and AGC Control Board. A new lead was installed. Other leads were checked for strength and dress and were found to be satisfactory.

System acceptance testing was resumed after environmental testing, and all test requirements were met.

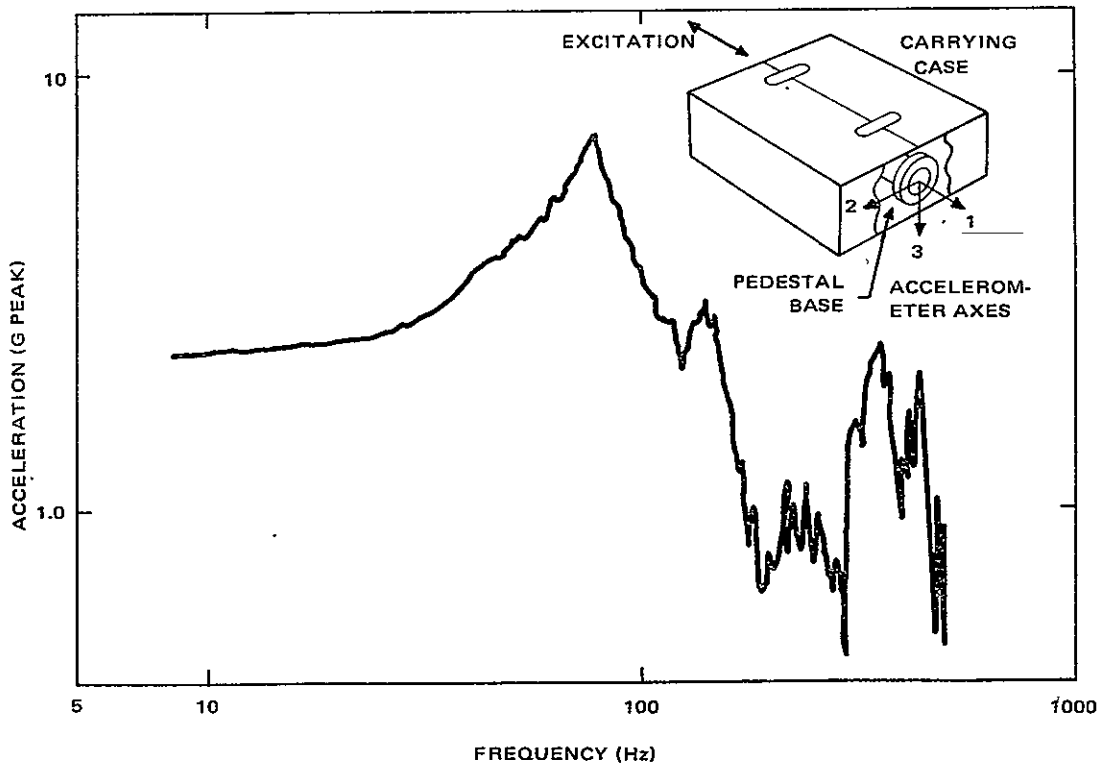

Figure V-1. Azimuth Axis Vibration Test (Accelerometer No. 1), Configuration and Vibration Level Curve

RCA | Defense Electronic Products | Astro Electronics Division | Princeton, New Jersey